Exploring Chemical Enhancement of Subcritical Fractures in Geomaterials

by

Manman Hu

Department of Civil & Environmental Engineering
Duke University

Date:_____

Approved:

_____
Tomasz A Hueckel, Supervisor

_____
Wilkins Aquino

_____
Guglielmo Scovazzi

Thesis submitted in partial fulfillment of
the requirements for the degree of
Master of Science in the Department of
Civil & Environmental Engineering in the Graduate School
of Duke University

2013

ABSTRACT

Exploring Chemical Enhancement of Subcritical Fractures in Geomaterials

by

Manman Hu

Department of Civil & Environmental Engineering
Duke University

Date:_____

Approved:

_____
Tomasz A Hueckel, Supervisor

_____
Wilkins Aquino

_____
Guglielmo Scovazzi

An abstract of a thesis submitted in partial
fulfillment of the requirements for the degree
of Master of Science in the Department of
Civil & Environmental Engineering in the Graduate School of
Duke University

2013

Copyright by
Manman Hu
2013

Abstract

Propagation of subcritical cracks is studied in a geomaterial subject to weakening by the presence of water, which dissolves a mineral component of it. Such weakening is common when tensile micro-cracks develop, constituting sites of an enhanced mineral dissolution. Meanwhile, the dissolution process at each active site of the inter-surface is affected by the chemical properties of the environment, e.g. the PH value. In this research, a previous concept of reactive chemo-plasticity is adopted with the yield limit depending on the mineral mass dissolved and causing a chemical softening. The dissolution is described by a rate equation and is a function of a variable internal specific surface area, which in turn is assumed to be a function of the dilative plastic deformation. Two loading modes are adopted to investigate the chemical enhancement of propagation of a single crack. The behavior of the material is rigid-plastic with a chemical softening. The extended Johnson approximation is adopted, meaning that all the fields involved are axisymmetric around the crack tip with a small, unstressed cavity around it. An initial dissolution proportional to the initial porosity activates the plastic yielding. The total dissolved mass diffuses out from the process zone, and the exiting mineral mass flux can be correlated with the displacement of the crack tip. A calibration against available data will be performed in the future, followed by a series of experiments to simulate the real case.

Dedication

To my parents, who raised me with loving care and made me who I am.

Contents

List of Figures

Acknowledgements

I would like to thank my advisor, Dr. Tomasz Hueckel sincerely for his guidance and encouragement that made this work possible. His insight, enthusiasm and devotion has always been a persistent source of inspiration during my research life.

I am also grateful to all of those who supported me in any aspect during my research at Duke University.

1. Introduction

1.1 Subject of the research

Chemically induced mass removal is encountered in many areas of geo-engineering, and often affects mechanical properties of the medium as well as its microscopic structure. In reality, a geo-material is often subject to a mechanical load, by nature (e.g. self-weight of soil/rock mass) or by human activities (e.g. applied forces). Its reaction to the load is affected when a portion of the mass in the medium is released via chemical dissolution. This specific mechanism of mass removal may lead to an enhanced micro-cracking process, which is believed to result in the overall material degradation. Though strain hardening may arise to compete with the chemical softening effect, which is often referred to as compensational mechanisms (Hu and Hueckel, 2007), the material is usually observed undergoing weakening. Meanwhile, the increased density of micro-cracks in the medium enhances chemical infiltration and mineral dissolution, which in turn affects the micro-cracking process. The coupling process occurs at multiple-scales, temporal and spatial, which adds to the complexity of this problem. The high non-linearity, unpredictability and variety of geological materials makes the modeling for the entire process intractable. However a better understanding of how an individual subcritical fracture propagates as a result of chemical enhancement is believed to be essential and achievable.

The assessment of the changes of mechanical properties, of strength (compressive, shear, or tensile) of geomaterials and of effective permeability of the medium as a function of the intensity and duration of the chemical exposure appears to be critical for reversal technology. Such assessment is suggested to be performed at several scales: (1) a micro-scale of a continuum in front of a macro-crack, known as process zone, where a series of micro-cracks exposed to chemical infiltration form, and propagate, weakening the material; (2) a meso-scale, at which individual macro-cracks propagate, as a result of the weakening of the process zone (see above); (3) a macro-scale, when changing the pattern of flow of fluids in such an evolving medium results in the evolution of macroscopic permeability, on one hand, and on the other a macroscopic mechanical properties.

This study focuses on the mechanisms of coupling between chemical processes (dissolution, precipitation and mass removal), mechanical properties and processes (material hardening/softening, chemo-plastic strain) and microstructure. These physical and chemical coupling effects appear to occur at all the three scales and also between the scales.

1.2 Motivations

In the past several decades, there has been a growing understanding that a number of problems in relationship to rock mechanics and rock engineering in general may or need to be tackled by addressing fracture mechanics. Many of the examples stem

from energy engineering and slope stability. The technique of hydraulic fracturing has been increasingly used all over the world due to its advantages in efficiently creating fractures in the rock formation, which dramatically enhances rock or sediment permeability and hence oil/gas production (Jackson et al., 2011; Rahman, 2008; Dershowitz et al., 2001). The application of hydraulic fracturing for enhancing oil recovery was apparently first recorded in 1947 in Kansas (Howard and Fast, 1970), and since then it has been intensely developing (Carter et al., 2000). Dershowitz et al. (2001) developed a multiphase discrete fracture model to show how water injection improves oil recovery in the Oregon Basin in Wyoming. More recently, the attention shifted towards fracture propagation enhancement by acidizing (i.e. injecting chemically active fluids), especially for low permeability carbonate reservoirs. The most recent examples include a study on the application of matrix acidizing to enhance a geothermal system (Zimmermann et al., 2010) in Germany, a Regular Mud Acid (RMA) stimulation being performed at Soultz Enhanced Geothermal System (EGS) reservoir in France (Portier and Vuataz, 2010), formation permeability being enhanced through shear fracturing due to well stimulation at an EGS in the Desert Peak geothermal field, Nevada (Lutz et al., 2010), as well as He et al. (2010)'s study on the wormholes by acidizing in tight carbonate reservoir, just to mention a few.

Meanwhile, there has also been a heated debate on acidizing treatment in hydraulic fracturing performance, due to the potential harm caused by disposal and

transport of the toxic wastewater, which may include formaldehyde, boric acid, hydrochloric acid, and isopropanol (Coffman, 2009). Poorly-controlled hydraulic fracturing, often due to inadequate understanding of fracture mechanisms involving acid-rock interaction, may not only pose threat to the environment, but also result in unnecessary costs and low productivity (Rahman, 2008). This investigation addresses the possible chemo-mechanical mechanisms of rock/shale weakening and resulting fracture propagation enhancement.

1.3 Background

1.3.1 Phenomenological Considerations on Coupling Between Mass Removal and Mechanical Damage

Coupling between chemistry and mechanics in rocks occurs and can be observed, measured and interpreted at several scales. In general, a mechanically stressed material in subcritical conditions can be brought to failure by mass removal either locally or at boundaries. As a consequence, there is less of the material to resist stress or the material becomes weaker, depending at which scale the process is observed. For instance, when crack propagation is considered in a geomaterial subject to weakening by the presence of dynamic water with or without an additional aggressive agent, the solid-fluid interphase becomes site, where a mineral removal occurs. The mass removal we investigate in this research is induced by the mineral dissolution in the course of a chemical reaction at the wall surface of micro-defects, which is often referred to as chemical mass removal. Other possible causes of mass removal, for example, dynamic

action of the pore-fluid moving with a velocity affecting mineral fines located between soil particles, are not considered in this study. Coupling mechanisms of chemical dissolution and irreversible strain has been investigated by Hu and Hueckel (2007 a, b) on the micro-indentation process, while this study expands this concept to a wider view concerning several industrial interests (e.g. slope stability, oil shale engineering and enhanced geo-thermal systems). The chemical and mechanical processes in these engineering applications are strongly coupled in several scales, and they both contribute to the coupling with other properties of the material (e.g. permeability). This study aims at further advancing the chemo-mechanical modeling with an emphasis on the coupling mechanisms between chemical mass removal and irreversible damage in the vicinity of the crack tip in subcritical situations, and thereafter getting a better understanding on the chemical enhancement of subcritical fractures.

1.3.2 Existing Framework of Chemo-plasticity

Solid-fluid interaction in geomaterials has been studied for many years focusing on the effect of pore pressure on rock or soil matrix. The concept of reactive chemo-plasticity is based on the notion that a mass removed from/added to a solid isochorically (without the volume change of the representative elementary volume of the porous medium) and adiabatically (without heat exchange) affects both the medium compliance and strength (Hueckel, 2002; Hu and Hueckel, 2007 a, b) as well as permeability (Hueckel and Hu, 2011). As one of the primary sources of mass removal, chemical

dissolution has been attracting much attention. A key mechanism that links the chemical process and mechanical degradation is micro-cracking. Bathust (1958) and Ostapenko (1968, 1975) noted that micro-cracking leads to the generation of new solid-fluid interface, where mineral dissolution takes place. Tada et al. (1987) found that micro fractures and plastic deformation play an important role in the process of pressure solution.

The concept of chemical dissolution coupled with plasticity was addressed in Hu and Hueckel' papers (2007 a, b), linking the irreversible dilatancy and the related increase of free specific surface area to the amount of mineral dissolution per unit volume, which in turn enhances the chemical weakening. This coupling mechanism, usually referred as "reactive chemo-plasticity", acts at a comparatively long time scale, distinguished from "non-reactive chemo-plasticity", i.e., when mechanical properties of solid skeleton can be affected instantaneously by the altered concentration (of selected species) in pore fluid.

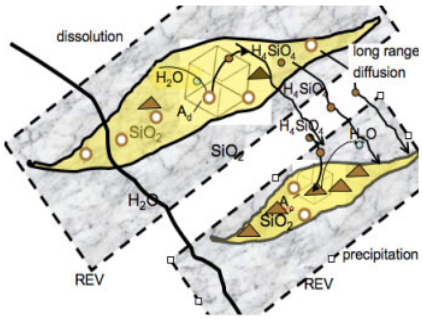

Figure 1: Diagram of mineral mass removal occurring at dissolution sites at micro-crack walls (from Hu and Hueckel, 2007a)

Observations of reactive chemo-plasticity start from a microscopic point of view when mineral mass dissolves into water at available dissolution sites on the solid-fluid interface. It is commonly assumed that the mass removal (dissolution reaction) rate is proportional to the specific surface area of the interface. It is hence postulated that the irreversible damage-induced dilatancy, is a good measure of the generation of new micro-crack walls. The increased micro-crack surface area adds to the pre-existing specific surface area of the innate pore solid-liquid interface per unit volume, hence enhancing the overall mass loss from the medium.

Since mass removal lowers the strength of the medium, i.e. produces chemical softening, an important part of description of the chemo-mechanical coupling is to quantify how much weaker the material becomes due to dissolution. Therefore, the coupling between the irreversible strain and the chemical reaction of mass removal is a two-way coupling (see also Hueckel and Hu, 2009).

It is assumed that the yield surface evolution is affected only by stress rate, and the rates of irreversible strain hardening as well as the internal variable of mass removal, ξ, which is accumulated dissolved mineral mass. At the yield surface, $f = 0, \dot{f} = 0$, the irreversible strain rate is obtained through the associated flow rule:

$$\dot{\varepsilon}_{ij}^{irr} = \dot{\Lambda}\frac{\partial f}{\partial \sigma_{ij}}$$

where the multiplier $\dot{\Lambda}$, can be expressed as a function of rate of stress and chemical reaction process:

$$\dot{\Lambda} = \frac{\frac{\partial f}{\partial \sigma_{ij}}\dot{\sigma}_{ij} + \frac{\partial f}{\partial \xi}\dot{\xi}}{-\frac{\partial f}{\partial \varepsilon_q^{irr}}\left[\frac{2}{3}\frac{\partial f}{\partial s_{kl}}\frac{\partial f}{\partial s_{kl}}\right]^{\frac{1}{2}}};$$

$$s_{kl} = \sigma_{kl} - \frac{1}{3}\sigma_{mn}\delta_{kl}$$

which is derived from the extended Prager's consistency condition:

$$f = f(\sigma_{ij}, \varepsilon_q^{irr}, \xi)$$

$$\dot{f} = \frac{\partial f}{\partial \sigma_{ij}}\dot{\sigma}_{ij} + \frac{\partial f}{\partial \varepsilon_q^{irr}}\dot{\varepsilon}_q^{irr} + \frac{\partial f}{\partial \xi}\dot{\xi} = 0$$

The yield locus gradient suggests the mode of strain rate, while the magnitude of strain rate is controlled by multiplier $\dot{\Lambda}$, which implies through its expression that chemical mass removal has the ability to affect the development of irreversible strain and vice versa, when external loading on the system is fixed.

The chemo-plasticity effects play a role at all scales and are a versatile tool to represent corresponding mechanics at those scales. At the micro-scale it is most prominent in the process zone in front of the crack-tip as it appears that it controls the process of crack propagation.

During the chemo-mechanical process, other properties of the soil/rock material, such as intrinsic permeability and porosity, in terms of hydraulic characteristics, are affected as well. Effective permeability of fractured rock media depends not only on the

interconnected cracks, but also inter-crack solid rock generalized transmissivity between adjacent unconnected cracks, especially when a large portion of fractures are non-connected. This transmissivity is a function of permeability of open cracks, intrinsic permeability of the rock matrix and the distance between adjacent crack tips. As a matter of fact, two neighboring cracks might function as "connected" if sufficient micro-channeling takes place between them. Such phenomena may become pronounced when the pre-fractured material is stressed and is subject to mass loss due to chemical dissolution or possibly hydro-erosion. As cracks propagate, the medium transmissity is most sensitive on the segments of lowest permeability, i.e. the area of solid matrix between two adjacent cracks. Removal and precipitation of mineral from the cracks themselves affects the permeability evolution (Hueckel and Hu, 2011).

2. Objectives and Tasks

The main objective of this study is to formulate a better understanding on the process of crack propagation in a geomaterial under both mechanical and chemical loading. The processes of these two types of loading are coupled in nature, developing within multiple scales, both spatial and temporal. The investigation will be carried out within the framework of chemo-mechanics theories and then followed by a series of experiments, which in turn reveal specific mechanisms of interactions and hopefully result in postulating of distinctive constitutive equations. Based on the chemo-plasticity theory that Hu and Hueckel (2007 a, b) applied to the micro-indentation process, we further investigate on circumstances of industrial interest that involve chemical enhancement of crack propagation, employing the concept that irreversible strain is coupled with mass removal. Numerical simulations will be performed for simplified scenarios based on developed models. Meanwhile, an experimental set up will be built to help understand the actual mechanisms and their models, with the numerically obtained solutions and parametric studies serving as a reference and for comparison.

Specific tasks to be undertaken includes:

- To establish the effects of micro-cracking in the process zone, with and without chemical enhancement.
- To establish quantitative relationships between variables controlling geochemical-mechanical coupling.

- To establish the coupling mechanisms between mass removal (i.e. chemical dissolution) and irreversible damage in the vicinity of a subcritical fracture.
- To perform a series of experiments that simulate the geo-chemically enhanced crack propagation as well as the alteration of overall hydraulic transmissivity.
- To analyze of the experimental results in light of the modeling results.
- To further adjust or improve the model, and repeat the previous step until reach certain degree of watch.
- To develop a model for linking the effective permeability to account for the dilatant deformation/damage and hence the irreversible strain.
- To compare findings from simulation results of different circumstances.
- To propose a general model for chemo-mechanical coupling in environmentally enhanced crack propagation.
- To further explore the process of mass removal, and its coupling with the mechanical and hydraulic properties in a system of fractures.

3. Concept of Chemo-plasticity

3.1 Coupling between Mass Removal and Plasticity

As one of the leading geo-environmental problems in the world, the mass removal phenomenon can be observed everywhere, affecting public health, safety, property and environment, costing construction industry and local government billions of dollars a year. The most significant consequences of mass removal include landslides, scour at the bridges, sand production in the oil recovery, etc. The process of mass removal is often coupled with chemical reactions occurring on the interface of two phases, i.e. the solid porous material and an aggressive fluid (e.g. acid rain in the cases of slope instability). The chemical mass release weakens the strength of the material, which meanwhile poses an influence on the mass dissolution rate via micro-structural alteration of the material. The mutually promoting effect between chemical reactions and mechanical weakening induces enhanced degradation in the medium.

Another concern on chemical mass removal that attracts enormous attention is from the energy field. Since the technique of hydraulic fracturing has been proved efficient in enhancing rock or sediment permeability and hence oil/gas production (Jackson et al., 2011; Rahman, 2008; Dershowitz et al., 2001) as well as heat extraction from geothermal fields (Portier and Vuataz, 2010; Zimmermann et al., 2011), the acidizing treatment which plays an essential role in the fracturing process has been intensely studied lately. The main purpose for acidizing (injecting chemically active

fluids) is to enhance fracture propagation and hence the effective permeability in the target reservoir. In such cases, the fractures created by perforating performance are filled with pressurized acid water. Under both the mechanical load and the chemical load, the material goes through a series of complex processes at the microscopic scale, where the coupling of the two types of loads is realized via micro-cracking process induced by mineral removal. While at the macroscopic scale, the alteration on mechanical properties of the reservoir material is of great concern as well, which might be a cause for local subsidence or uneven settlement.

There are typically two types of mass removal. One is due to the mineral release caused by a chemical reaction at the wall surfaces of micro-defects, which has been studied in the papers of Hu and Hueckel (2007 a, b). The other one is due to dynamic action on grains of pore-fluid moving with a velocity affecting filling fine minerals between soil grains, and weakening grain-matrix interface. Little is known on its inside mechanisms. However, these two effects are usually coupled together as a mutually enhancing action of chemistry and fluid dynamics, which has not been addressed before.

3.2 Mechanics of Chemical Mass Removal

Solid-fluid interaction in geomaterials has been studied for many years focusing on the effect of pore pressure on rock and soil matrix. The concept of reactive chemo-plasticity is based on the notion that a mineral mass removed from/added to a solid can affect both the medium compliance and strength (Hueckel, 2002, Hu and Hueckel,

2007a, b). As one of the primary sources of mass removal, chemical dissolution has been attracting much attention. A key mechanism that links the chemical process and mechanical degradation has known for sometime to be rock micro-cracking. Bathust (1958) and Ostapenko (1968, 1975) noted that micro-cracking leads to the generation of new solid-fluid interface, where an enhanced mineral dissolution takes place. Tada et al. (1987) found that micro fractures and plastic deformation play an important role in the process of pressure solution.

The concept of chemical dissolution coupled with plasticity was addressed in Hu and Hueckel' papers (2007a, b), linking the irreversible dilatancy and the related increase of free specific surface area to the amount of mineral dissolution per unit volume. This coupling mechanism, usually referred as "reactive chemo-plasticity", acts at a comparatively long time scale, distinguished from "non-reactive chemo-plasticity", i.e., when mechanical properties of solid skeleton can be affected instantaneously by an altered concentration (of selected species) in the pore fluid.

From a microscopic point of view reactive chemo-plasticity starts when a mineral mass dissolves into water at available dissolution sites on the solid-fluid interface. It is commonly assumed that the dissolution reaction rate and hence mass removal rate is proportional to the specific surface area of the interface. It is hence postulated that the irreversible damage-induced dilatancy, is associated with the generation of new micro-crack walls. The increased wall surface area adds to the pre-existing specific surface area

of the pores, hence advancing the overall mineral mass production of the medium. Since mass removal affects the strength of the medium, the central part of the description of the chemo-mechanical coupling is how to quantify how much weaker the material becomes due to dissolution. Therefore the coupling between the irreversible strain and the chemically induced mass removal is a two-way coupling (see also Hueckel and Hu, 2009).

To quantify the above coupling mechanisms, a Representative Elementary Volume (REV) of the drained porous medium is considered, represented by a single geometrical point, to which both mechanical and chemical properties are attributed. The solid phase material is assumed as rigid-plastic. This assumption is a matter of convenience, as it makes it possible to obtain a semi-analytical solution. On the other hand the elastic stress component is much smaller than the irreversible one in the area of interest near the crack tip. The partial stress carried by the fluid phase carries is considered negligible. The theory of plasticity states that the yield locus of a material is affected by stress σ_{ij} and when a sufficient load is applied that induces initial yielding, also due to variation of a set of internal variables. In reactive chemo-plasticity (Hueckel, 2002), the internal chemical variables denoted as $\xi_n, (n = 1,2,\dots)$, are the accumulated dissolved masses of the nth species of mineral per unit volume of the porous medium. The mechanical, strain-hardening variable is chosen as irreversible deviatoric strain intensity (ε_q^{irr}).

The rate of the deviatoric strain intensity is defined as an invariant of deviation strain rate $\dot{e}_{ij}^{irr}$:

$$\dot{\varepsilon_q}^{irr} = (\frac{2}{3}\dot{e}_{ij}^{irr}\dot{e}_{ij}^{irr})^{1/2},$$
$$where\ \dot{e}_{ij}^{irr} = \dot{\varepsilon}_{ij}^{irr} - \frac{1}{3}\dot{\varepsilon}_{kk}^{irr}\delta_{ij} \quad (1)$$

With the assumption of rigid-plasticity, there is no elastic strain rates and no strain at all for a stress state below the yield limit, i.e. when $f(\sigma_{ij}) < 0$. With the stress at the yield locus, the strain rate is nonzero and irreversible. Hence:

$$f = f(\sigma_{ij}, p_c),\ and\ \dot{f} = \dot{f}(\dot{\sigma}_{ij}, \dot{p_c}); \quad (2)$$

$$\dot{\varepsilon}_{ij} = 0\ when\ f < 0,\ or\ f = 0,\ \dot{f} < 0; \quad (3)$$

$$\dot{\varepsilon}_{ij} = \dot{\varepsilon}_{ij}^{irr} \neq 0\ when\ f = 0\ and\ \dot{f} = 0 \quad (4)$$

where the superimposed dot over a symbol denotes the time rate. Tensile stress and strain are considered as negative. p_c denotes a geometric size characteristics of the yield locus, and it plays the role of the hardening function of irreversible deviatoric strain (ε_q^{irr}) and of the accumulated relative dissolved mass of each mineral species ($\xi_1, \ldots, \xi_n$), hence $p_c = p_c(\varepsilon_q^{irr}, \xi_1, \ldots, \xi_n)$. During the process of dissolution, the material gets chemically softened at the condition that there is dilatant micro-cracking; on the other hand plastic deviatoric strain induces the hardening effect. This indicates that the two factors, plastic deviatoric strain and chemical softening, affect the yield locus of the material with the opposite contribution. At an imposed constant stress at yielding, the

plastic deviatoric strain hardening compensates for the dissolution induced strength loss.

The chemical softening parameters, $(\xi_1, \ldots, \xi_n)$, representing the accumulated mass removal of each particular mineral species can be calculated from the rates of reactions in which the given species is involved. In reality, multiple reactions may affect the strength of any geomaterial, the processes of which might be simultaneous or sequential with varied progressing rates or within different time scale. However, there is currently no widely accepted approach to identify and quantify contributions of individual mineral components to the overall degradation of material strength or other mechanical properties. Meanwhile, it is common that one type of chemical reaction is predominant, as in for instance, carbonate reservoirs subjected to acid environment, or calcite exposed to water (Ciantia and Hueckel, 2013). In what follows, a single reaction effect with a single rate will be considered only, and the chemical softening parameter becomes the reaction progress variable ξ, and hence, $p_c = p_c(\varepsilon_q^{irr}, \xi)$. The mechanisms of chemically induced mass removal will be detailed in the following section.

The irreversible strain rate can be obtained through the associated flow rule:

$$\dot{\varepsilon}_{ij}^{irr} = \dot{\Lambda} \frac{\partial f}{\partial \sigma_{ij}} \tag{5}$$

where the multiplier $\dot{\Lambda}$, can be expressed as a function of rate of stress and chemical reaction process:

$$\dot{\Lambda} = \frac{\frac{\partial f}{\partial \sigma_{ij}}\dot{\sigma}_{ij} + \frac{\partial f}{\partial \xi}\dot{\xi}}{-\frac{\partial f}{\partial \varepsilon_q^{irr}}\left[\frac{2}{3}\frac{\partial f}{\partial s_{kl}}\frac{\partial f}{\partial s_{kl}}\right]^{\frac{1}{2}}}; \tag{6}$$

$$\dot{\Lambda} = 0 \; if \; f < 0 \; or \; f = 0 \; and \; \dot{f} < 0$$

is determined via the extended Prager's consistency law, $\dot{f}(\sigma_{ij}, \varepsilon_q^{irr}, \xi) = 0$. The yield locus gradient $\frac{\partial f}{\partial \sigma_{ij}}$ determines the mode of strain rate, while the magnitude of strain rate is controlled by multiplier $\dot{\Lambda}$, which implies that a purely chemical process can promote the development of irreversible strain when stress is fixed (see Hu and Hueckel, 2007a, b for details).

4. Approaches to Simulate Crack Propagation

4.1 Mechanism of Mineral Dissolution Coupled with Volumetric Strain

As one of the two major reservoir lithotypes, carbonates (the other are sandstones) have been intensely studied in the petroleum industry (Dusseault, 2011). The most common chemical process in carbonate reservoirs is the dissolution of calcite and dolomite (André et al., 2007). Since the dissolution of dolomite, described as $CaMg(CO_3)_2 + 2H^+ \leftrightarrow Ca^{2+} + Mg^{2+} + 2HCO_3^-$, is found to be geochemically similar to calcite, we discuss calcite dissolution as a representative for carbonate minerals in general. When subjected to low concentration acid aqueous environment, calcite undergoes the predominant reaction described as:

$$CaCO_3(s) + H^+(aq) \leftrightarrow Ca^{2+}(aq) + HCO_3^-(aq) \tag{7}$$

This is usually the first step of the calcite-water interaction; the product HCO_3^- formed in aqueous solution is unstable, and inclines to convert to $CO_2(g)$ with the presence of excessive H^+. However, since it is the most significant reaction involved in solid mass removal, we believe to be acceptable to omit the subsequent reactions and consider reaction (7) as the dominant and hence the only reaction. Based on the mass conservation of calcium, the mole number of calcite removed from the solid phase ($CaCO_3$) is equal to the change in number of calcium ions in the solution, and the reaction rate is expressed as:

$$\frac{da_{Ca^{2+}}}{dt} = \tilde{A}\gamma_{Ca^{2+}}(k_+ a_{CaCO_3} a_{H^+} - k_- a_{Ca^{2+}} a_{HCO_3^-}) \tag{8}$$

where $\tilde{A}$ is a non-dimensional quantity denoting the total fluid-solid interface surface area per unit volume; a_i are activities and γ_i are activity coefficients of ith species; k_+ and k_- are rate constants of forward and backward reactions, respectively.

The rate of calcite removal from the solid phase of carbonate material can be represented by the rate of change of activity of Ca^{2+} in pore water, written as

$$\dot{\xi} = s\frac{da_{Ca^{2+}}}{dt} \tag{9}$$

where s denotes a ratio between the number of moles of water and that of calcite in the initial state. To maintain the linearity of our model, the precipitation term in Eqn. (8) is omitted.

Scalar variable $\tilde{\alpha}$ is introduced to represent a normalized amount of the increased surface area per unit volume of the medium, which is linked to the dimensionless total reactive surface area per unit volume of fluid (denoted by $\tilde{A}$) via $\tilde{\alpha} = \tilde{A}\frac{n\rho_w}{\rho^0}$, where $\rho^0 = 1kg/m^3$, ρ_w is the density of water and n denotes porosity taken at its initial value.

The newly generated specific surface area can be assumed as proportional to the irreversible dilatant volumetric strain, as suggested by a model of a two-dimensional hexagonal crystal assembly (Hu and Hueckel, 2007b). Then we have $\tilde{\alpha} = 8/(\sqrt{3}\delta)|\varepsilon_v^{irr}| \cdot 1m$ for $\varepsilon_v^{irr} < 0$, where δ denotes an average micro-crack opening at the apex. Hence,

$$\tilde{A} = f(\varepsilon_v^{irr}) = \phi|\varepsilon_v^{irr}| + \phi_c, \;\; \varepsilon_v^{irr} < 0 \tag{10}$$

$$\phi = 0, \ \varepsilon_v^{irr} > 0 \tag{11}$$

where ϕ is a proportionality constant, ϕ_c denoting the dimensionless specific surface area of the pre-existing voids per unit volume. When the volumetric strain is compressive, it is assumed that there is no micro-cracking and that the specific surface area remains constant.

4.2 Remote Traction Mode

There are several circumstances of industrial interest involving the chemical enhancement of crack propagation. One typical scenario features a remote constant radial tensile stress, which goes to zero at the inner (artificial) boundary of the process zone, r = a. At the same time, yielding which induces irreversible deviatoric strain is localized near crack tip, producing also a proportional amount of irreversible dilatancy (meaning micro-cracking). The latter induces the chemical mass removal enhanced by its rate dependence. Due to the chemical action of the fluid, the material weakens in that zone. The circumferential stress is also tensile everywhere. Due to boundary constraints the stress state does not evolve significantly, and hence the whole process is dominated by compensation of the chemical softening by the strain hardening (Hueckel, 2009).

From the field point of view, in this scenario the chemical effect plays a primary role, while the stress field plays a secondary role. It corresponds to a situation of a pre-existing crack inundated with water or an aggressive liquid (e.g. acid rain), while a

tensile stress source is remote. A possible field analogue could be a reactivation of a landslide with a pre-existing slip zone (see eg. Zhao et al., 2011).

Classically, a mechanically stimulated crack extends when a sufficiently high level of stress intensity is attained in the material at the crack tip. The micro-cracking can macroscopically be represented through the inelastic strain near the crack tip and its yielding affected by the strain softening. In contrast, in the considered case, the external tractions are kept constant, while the process is activated and driven via the chemical field.

To address the solution of the boundary value problem for the system of equations describing the coupled chemo-mechanical processes around the crack tip we adopt the extended Johnson approximation (Johnson, 1970), assuming that all the fields involved are axisymmetric around the crack tip point with a small, unstressed cavity around it, as shown in **Figure 2**. This is analogous to the cylindrical cavity expansion problem often used for pile or piezocone modeling in geotechnical problems (see e.g. Collins and Stimpson, 1994 or Bigoni and Laudiero, 1989). For simplicity, the plane strain is considered. The boundary conditions impose the radial stress at the external boundary as constant and uniform, and zero at the inner boundary:

$$\sigma_r|_{r=a} = 0; \;\; \sigma_r|_{r=b} = const. \tag{12}$$

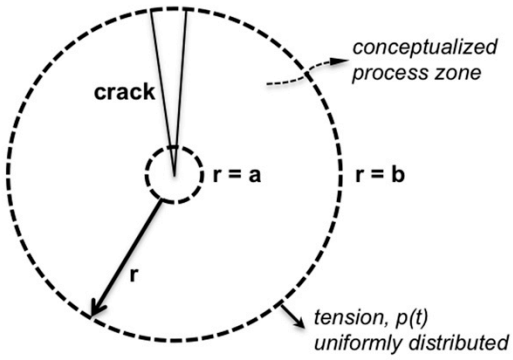

Figure 2: Schematic diagram of the process zone around tip of a crack

Note that other boundary conditions that one normally would impose on a boundary value problem as shown in **Figure 2**, like zero circumferential stress at the crack faces, are ignored by virtue of adopting the Johnson approximation, that allow one to use the axial symmetry fields. While notably the obtained solutions are not exact, the benefit from capturing principal interrelationships between the variables involved and their distribution and evolution is significant. Note also, that assuming zero radial stress at the inner boundary excludes any realistic description of the stress concentration near the crack tip. However, our focus is rather on the adjacent process zone of microcracking, which is away from the crack tip by a non-negligible distance, represented in our case by the radius *a.* (Bazant and Kazemi, 1990, Lin and Labuz, 2011).

The equilibrium equation and kinematic relationships for the plane strain axisymmetric problem are given as:

$$\frac{d\sigma_r}{dr} + \frac{\sigma_r - \sigma_\theta}{r} = 0; \;\; \dot{\varepsilon}_r = -\frac{d\dot{u}}{dr}, \;\; \dot{\varepsilon}_\theta = -\frac{\dot{u}}{r}, \;\; \dot{\varepsilon}_z = 0 \qquad (13,14)$$

where θ and r denote the circumferential and radial coordinates (respectively), and u, denoting a radial displacement are defined as positive when pointing outwards. The circumferential displacement is null due to axisymmetry.

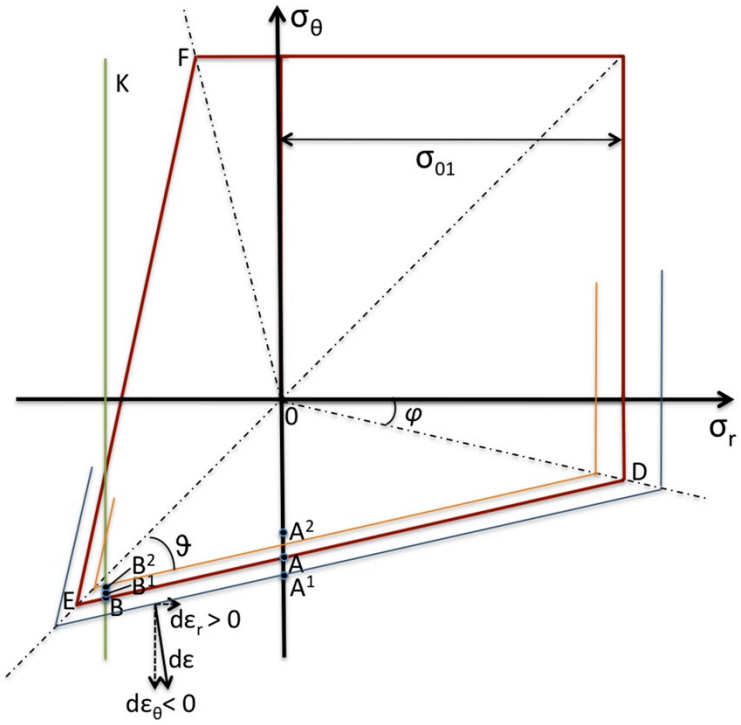

(a)

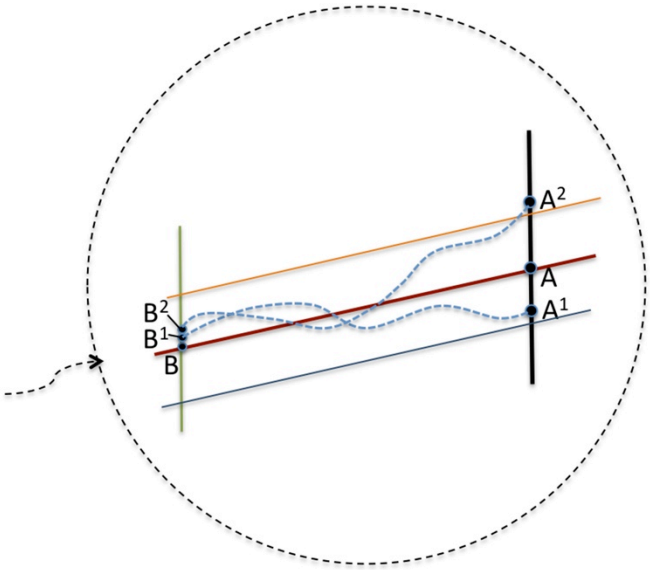

(b)

Figure 3: (a) Linearized yield locus for the material; (b) Sketch of stress profiles within the process zone

A linearized yield surface is chosen for simplicity after Mróz and Kwaszczynska (1971), Hueckel and Mróz (1973), as shown in **Figure 3a**. Tensile stress or strain is considered negative in the present system, hence, the process of yielding starts from the third quadrant in **Figure 3a**. The locus segment ED determines the relationship between σ_r and σ_θ at the initial yielding: $\sigma_{\theta 0} = tan(\frac{\pi}{4} - \vartheta)\sigma_{r0} - (tan(\frac{\pi}{4} - \vartheta) + tan\varphi)\sigma_{01}$, where ϑ, φ and σ_{01} are parameters shown in **Figure 3a.** The linearized yield locus undergoes an expansion with an increase of the shear strain intensity (Eqn. 1), while it shrinks with the square of the loss of the mineral mass, ξ. The assumed hardening rules are:

$$\sigma_r = \sigma_{r0}(1 + \alpha\varepsilon_q^{irr} - \beta\xi^2); \tag{15}$$

$$\sigma_\theta = tan(\frac{\pi}{4} - \vartheta)\sigma_r - (tan(\frac{\pi}{4} - \vartheta) + tan\varphi)\sigma_{01}(1 + \alpha\varepsilon_q^{irr} - \beta\xi^2) \tag{16}$$

One should notice that Eqn. (15) and Eqn. (16) apply exclusively for $\sigma_\theta < \sigma_r < 0$. α and β are constant coefficients for strain hardening and chemical weakening, respectively. Deviatoric strain intensity ε_q^{irr} can be calculated via Eqn. (1) integrated with time. The axial stress component σ_z is assumed not to influence yielding in the plane strain rate conditions. It can be calculated through Eqn. (5) from the condition $d\varepsilon_z^{irr} = 0$ as, $\sigma_z = \frac{1}{2}(\sigma_r + \sigma_\theta) \pm 3BJ_2^{1/2}$, where B is a constant and J_2 is second invariant of deviatoric stress, while the sign $\pm$ refers to either top or the bottom part of the yield locus, **Figure 3a**, (see also Mróz and Kwaszczyńska, 1971).

Recall that we neglected the precipitation effect. Hence the combination of Eqn. (8) and Eqn. (9) yields:

$$\dot{\xi} = s\tilde{A}\gamma_{Ca^{2+}}k_+a_{CaCO_3}a_{H^+} \tag{17}$$

We further assume the activities and activity coefficients are unities for the convenience of simulation, and hence $\dot{\xi}$ can be rewritten as

$$\dot{\xi} = sk_+(\phi|\varepsilon_v| + \phi_c), \ \ \varepsilon_v < 0 \tag{18}$$

Hence, if ε_v is negative,

$$\beta\xi^2 = \beta(\int_0^t \dot{\xi}\, dt)^2$$
$$= \beta s^2 {k_+}^2(\phi \int_0^t |\,\varepsilon_v| dt + \phi_c t)^2, \tag{19}$$

which leads to

$$\beta\xi^2 = K^2(\int_0^t |\,\varepsilon_v| dt)^2 + 2KK_c t(\int_0^t |\,\varepsilon_v| dt) + {K_c}^2 t^2, \tag{20}$$

where $K = \sqrt{\beta} s k_+ \phi$, $K_c = \sqrt{\beta} s k_+ \phi_c$, representing the overall chemical softening rate coefficients associated with newly generated micro-cracking and the initial void ratio, respectively.

An initial dissolution, proportional to a constant specific surface area associated with the initial porosity, even for a low stress prior to yielding, i.e. for σ_{ij}: $f = f(\sigma_{ij} = const., \xi = \frac{K_c}{\beta} t) < 0$ through a slow mass removal $\dot{\xi} > 0$ and corresponding shrinkage of the yield locus can eventually activate the plastic yielding at ED (**Figure 3**) i.e. bring the condition $f = 0$ around the initially subcritical crack. At that point, with the continuing reaction, $\dot{\xi} > 0$, but now also enhanced by the micro-cracking as manifested by $\dot{\varepsilon}_v > 0$, the coupled process is significantly intensified.

4.3 Hydraulic Pressurizing Mode

Another scenario of our interest can be described as a single crack being affected by the pressure of the fluid acting on the walls of the crack (as shown in **Figure 4**), and at the same time by a chemical infiltrating from the crack and weakening the crack surroundings. No other load is considered. The action of the pressure transmitted to the rock causes dilatant damage near the crack tip and hence engages the chemo-mechanical coupling in that location. The stress state near the crack tip is different from the one described in the previous section in the fact that the stress near the crack tip is compressive orthogonally to the crack edges. On contrary to the previous scenario, in this case both factors, chemical and mechanical, are equally important. Such case is likely to occur during fluid pressure (static) pulse assisted by the chemically aggressive fluid component.

In order to avoid singularity at the very tip, we consider a small rounded cavity instead of a single point, and thereafter the stress distribution pattern at the crack-tip surface is obtained (see detailed part in **Figure 4**). The stress at the crack-tip is profoundly significant due to stress concentration, and a crack extends from its tip when a sufficiently high level of stress intensity is attained in the material. Since the crack is assumed narrow enough and the stresses at the walls are much less important compared to that at the tip, we again further adopt the extended Johnson approximation (Johnson, 1970), which amounts to the cylindrical cavity expansion problem often used for pile or

piezocone modeling in geotechnical problems (examples can be found in the papers of Collins and Stimpson, 1994 or Bigoni and Laudiero, 1989).

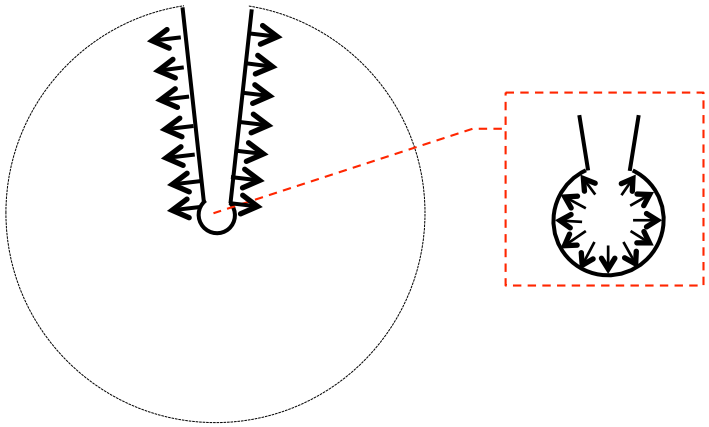

Figure 4: Mechanical sketch at the crack walls and detains at the crack-tip

In this approximation all the fields involved are assumed axisymmetric around the crack tip point with a small cavity around it, which simplifies our case to be as displayed in **Figure 5**. Since it has been demonstrated that the fracture toughness of soil is not affected by thickness of the specimen (Schmidt, 1980), plane strain is considered, confining the problem within 2-D configuration. The boundary conditions impose the radial stress at the inner boundary of the disk as constant and uniform, and zero at the external boundary:

$$\sigma_r|_{r=a} = P_a\ (const.); \qquad \sigma_r|_{r=b} = 0 \tag{21}$$

Note that other boundary conditions that one normally would impose on a boundary value problem as shown in **Figure 5**, like zero circumferential stress at the crack faces, are ignored in this case by virtue of adopting the Johnson approximation, that allow to use the axial symmetry fields. While notably the obtained solutions are not

exact, the benefit from capturing principal interrelationships between the variables involved and their distribution and evolution is significant.

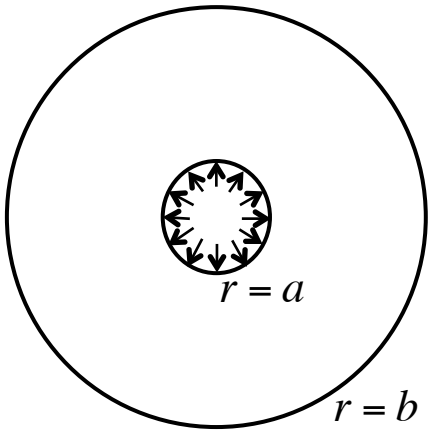

Figure 5: Sketch of the process zone after adopting extended Johnson Approximation (1970).

The equilibrium equation and kinematic relationships for the plane strain axisymmetric problem in this case is the same as what is given in Eqn. (13, 14).

A linearized yield surface is chosen for simplicity, as shown in **Figure 6**. Tensile stress or strain is considered negative in the present system, hence, the process of yielding starts from the 4th quadrant in **Figure 6**. The locus segment BD determines the relationship between σ_{r0} and $\sigma_{\theta 0}$ at the initial yielding: $\sigma_{\theta 0} = tan(\frac{\pi}{4} - \vartheta)\sigma_{r0} - (tan(\frac{\pi}{4} - \vartheta) + tan\varphi)\sigma_{01}$, where ϑ, φ and σ_{01} are denoted in **Figure 3**.

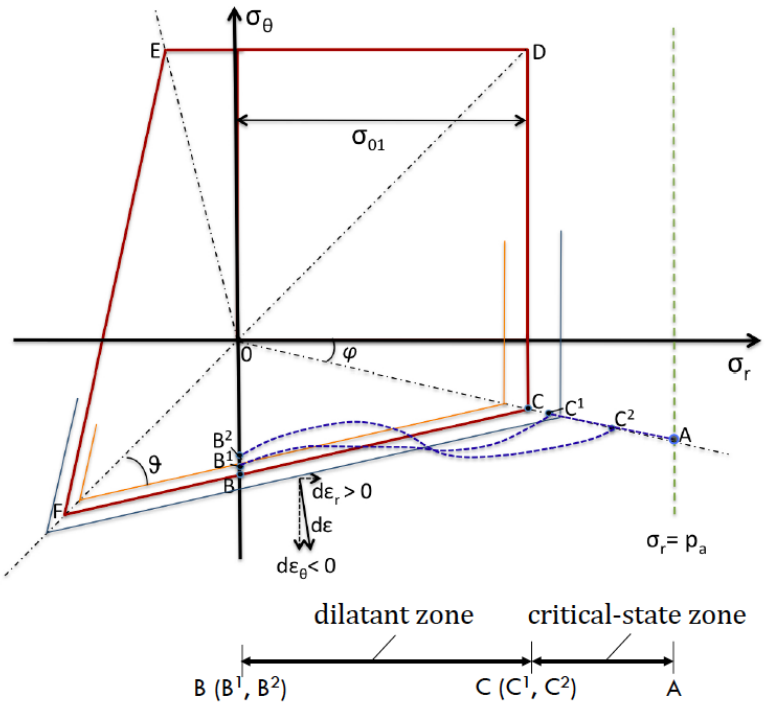

Figure 6: Sketch of the linearized yield locus and stress profiles

After a few calculations, P_a is determined at a value greater than σ_{01}, and the line that features $\sigma_r = P_a$ is set aside the yield locus in **Figure 6**. Given that the stress state of $r = b$ is fixed at the intersection of line FC (evolving in the process) and the y-axis, while that of $r = a$ has to reach $\sigma_r = P_a$ (see **Figure 6**), we come up with the two-zone model as shown in **Figure 7**. The inner one is named critical-state zone, within which the stress state of material is assumed moving along line CA in **Figure 6**. In the dilatant zone, during evolution process where hardening/softening may occur, σ_r and σ_θ can be correlated by:

$$\sigma_\theta = tan\left(\frac{\pi}{4} - \vartheta\right)\sigma_r - \left(tan\left(\frac{\pi}{4} - \vartheta\right) + tan\varphi\right)\sigma_{01} * (H + 1) \quad (22)$$

where H denotes the hardening parameter, which is defined as:

- If the material becomes harder, $H > 0$ (i.e. the yield locus expands);
- If the material becomes softer, $H < 0$ (i.e. the yield locus shrinks);
- If the strength of material does not change, $H = 0$ (i.e. the yield locus stays).

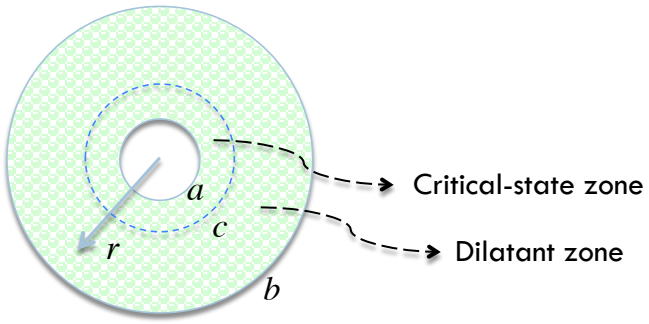

Figure 7: Sketch of the two-zone model

Continuity between the two zones require that

$$\sigma_r^{inner}\big|_{r=c} = \sigma_r^{outer}\big|_{r=c} \quad (23)$$

According to the concept of chemo-plasticity addressed by Hu and Hueckel (2007a,b), the hardening rule can be assumed linear as:

$$H = \alpha\varepsilon_q^{irr} - \beta\xi \quad (24)$$

where α and β are constant coefficients for strain hardening and chemical weakening, respectively. Deviatoric strain ε_q^{irr} is selected as a representative for the effect of hardening and its rate can be related with the rate of displacement through Eqn. 14 and

the relationship that $\dot{\varepsilon_r} = -\dot{\varepsilon_\theta} tan\left(\frac{\pi}{4} - \vartheta\right)$, observed from **Figure 6**. ξ denotes the loss of mineral mass, representing the softening effect. Hence, the increase of shear strain and the chemically induced mass loss are competing for making the material harder or softer.

The axial stress component σ_z is assumed not to influence yielding in plane strain rate conditions. It can be calculated through from the condition $d\varepsilon_z^{irr} = 0$ as, $\sigma_z = \frac{1}{2}\left(\sigma_r + \sigma_\vartheta\right) \pm 3BJ_2^{1/2}$, where B is a constant and J_2 is second invariant of deviatoric stress, while the sign $\pm$ refers to either top or the bottom part of the yield locus (in **Figure 6**), (Mróz and Kwaszczyńska, 1971).

If we adopt the hexagonal crystal assembly model (Hu and Hueckel, 2007b) and neglect the precipitation effect, the rate of mass removal can eventually be expressed as:

$$\dot{\xi} = K \int |\varepsilon_v^{irr}| \, dt + K_c t \tag{25}$$

Assuming the hardening rule is linear, then we have:

$$H = \alpha \varepsilon_q^{irr} - K \int \left|\varepsilon_v^{irr}\right| dt - K_c t \tag{26}$$

where ε_v^{irr} denotes the irreversible volumetric strain and is a function of avariable internal specific surface area. K and K_c represent the overall chemical softening rate coefficients associated with newly generated micro-cracking and the initial void ratio, respectively. An initial dissolution, proportional to a constant specific surface area associated with the initial porosity, even for a low stress, through a slow mass removal and corresponding shrinkage of the yield locus can eventually activate the plastic

yielding i.e. bring the condition *f = 0* around the initially subcritical crack. At that point, with the continuing reaction, $\dot{\xi} > 0$, but also enhanced by the micro-cracking as manifested by $\dot{\varepsilon}_v > 0$, the coupled process is significantly intensified.

The next step is to solve Eqns. 21~26. After a few steps of analytical derivation, eventually we get a system that contains only two nonlinear equations:

$$\begin{aligned}&(1-K_c t)\cdot(A_1 c^{ta-1}-A_2)-(\gamma u_c c^{ta}-K(1-ta)\int u_c c^{ta}dt)\cdot(A_3 c^{ta-1}-A_4 c^{-ta-1})-P_a\cdot c^{-1-\tan\varphi}=0\\&(1-K_c t)\cdot(B_1 c^{ta-1}-B_2)-(\gamma u_c c^{ta}-K(1-ta)\int u_c c^{ta}dt)\cdot(B_3 c^{ta-1}+B_4 c^{-ta-1})+\tan\varphi\cdot P_a\cdot c^{-1-\tan\varphi}=0\end{aligned}$$

(27)

where A_i, B_j $(i, j = 1, 2, 3, 4)$ can be calculated, and K_c, K, γ, ta, tanφ shall be prescribed.

Two methods are considered to solve this system of equations. The first one is to rewrite Eqn. 27 as:

$$\begin{aligned}&(1-K_c t)\cdot(A_1 d_1^{ta-1}-A_2)-A_3 d_1^{ta-1}d_2+A_4 d_1^{-ta-1}d_2-P_a\cdot d_1^{-1-\tan\varphi}=0\\&(1-K_c t)\cdot(B_1 d_1^{ta-1}-B_2)-B_3 d_1^{ta-1}d_2-B_4 d_1^{-ta-1}d_2+\tan\varphi\cdot P_a\cdot d_1^{-1-\tan\varphi}=0\end{aligned}$$

(28)

where

$$d_1 = c$$

$$d_2 = M = \gamma u_c c^{ta} - K(1-ta)\int u_c c^{ta}dt$$

In the *i*th time step, given $M(i)$, $M(i-1)$, $c(i)$, $c(i-1)$ and $u_c(i-1)$, $u_c(i)$ is obtained:

$$u_c(i) = \frac{M(i) - M(i-1) + (\gamma + K(1-ta)dt/2)\cdot u_c(i-1)\cdot c^{ta}(i-1)}{(\gamma - K(1-ta)dt/2)\cdot c^{ta}(i)}$$

(29)

Newton-Raphson iteration is performed in each time step with false position searching incorporated.

The second method serves as a check for the first one, and it can be summerized as:

- Obtain the equation with single unknown $\mathrm{c}(i)$, i.e. eliminating $M(i)$;
- Use MatLab function 'fzero' to calculate $\mathrm{c}(i)$;
- Then substitute $\mathrm{c}(i)$ back and get $M(i)$;
- Calculated $\mathrm{u_c}(i)$ with the same approach mentioned above in the Method I.

5. Preliminary Results

5.1 Preliminary Results from Remote Traction Mode

Numerical solutions were obtained by solving (using *Matlab* ©) the above-mentioned system of equations, given the initial and boundary conditions, as specified earlier. The input parameters are $\alpha = 1$, $\beta = 1$, $\vartheta = \pi/6$, $tan\varphi = 0.2$, $b/a = 10$, $K_c = 2.0\times10^{-8}s^{-1}$, and K is set to be $5.0\times10^{-6}s^{-1}$, unless it is a subject of a parametric study. The displacement u_a at the internal circumference is used to represent of the propagation of the crack tip, and its dimensionless form u_a/a as shown in **Figure 8**. If the value of chemical softening coefficient K, is increased by one order of magnitude, the displacement u_a within 1 month (30 days) starts growing exponentially, meaning an accelerated crack propagation, which is an expected result of the damage-dissolution coupling. **Figure 9** further demonstrates the relationship between the crack propagation as represented by u_a/a and a total integrated dissolved mass $\frac{1}{b-a}\int_a^b \int_0^t \dot{\xi}\, dtdr$. Notably, within the range studied at an advanced mass removal, a decelerating crack propagation is observed for a sufficiently high valued K. As seen also, for the same accumulated mass of dissolution, a smaller chemical coefficient K leads to a deeper crack penetration, as $\dot{\xi}$ is proportional to K and ε_v^{irr}, while the latter is linked to u_a. The evolution of the distribution of relative mass dissolution as well as of dissolution rate is shown in **Figure 10** and **Figure 11**, respectively. **Figure 10** indicates that the evolution of the accumulated dissolved mass distribution along the radius is confined to the near crack tip area. The

maximum accumulated relative mass removal reaches 0.67, which is very high. Note, that dissolution of carbonate rock can be very fast and advanced (see e.g. Ciantia and Hueckel, 2013). The confinement to the near-tip zone is even sharper in the dissolution rate distribution, as **Figure 11** demonstrates that the rate of chemical dissolution in the inner area of the process zone undergoes a huge change, while that outside of the area, it is almost negligible, as it comes mainly from the pre-existing surface area of the initial porosity. The rate distribution is clearly linked to that of dilatancy, along the radius, which (as shown in **Figure 12**) develops in a similar fashion, indicating that the near crack-tip area is subject to most severe damage. Given the linear form of the yield locus, and the normality rule, there is no compaction in the process zone. **Figure 13** and **Figure 14** show the evolution of the radial and circumferential stress component distribution, respectively. Because the radial stresses on both the interior and exterior boundaries are fixed, there is little freedom for any evolution. However, the distribution of σ_θ undergoes a noticeable change, specifically from t = 550h to t=1100h, during which the crack penetrates almost ten times deeper (as observed in **Figure 8**). It is interesting to notice that in the near crack-tip area the tensile (negative) stress experiences a small increase before it collapses back, which indicates an initially dominating strain-hardening followed by the progressive overtaking by the chemical softening. This is visible at the stress profiles for two representative moments in the evolution delineated in **Figure 3**, where A^1, A^2 stand for stress state at the interior, $r = a$, while

B^1, B^2 represent the counterpart exterior, $r = b$, respectively. The exterior of the process zone is subjected to consistent but much more modest chemical weakening mainly linked to the background dissolution as the deformational effect is very small.

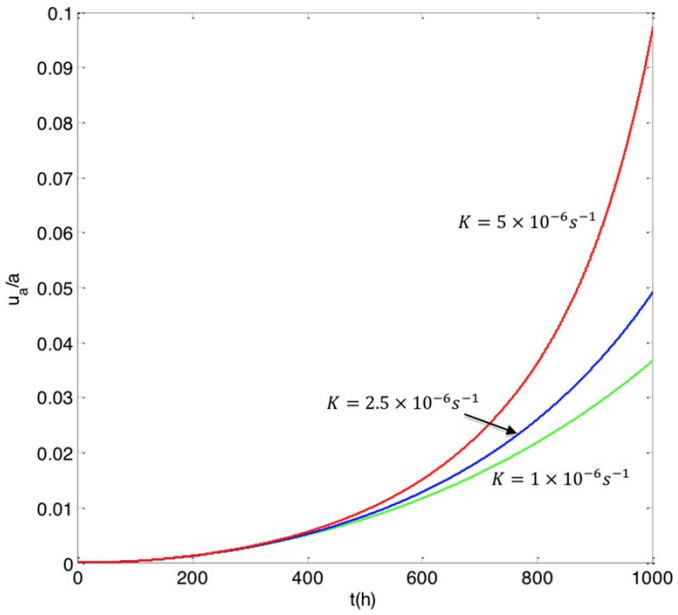

Figure 8: Propagation of the crack tip

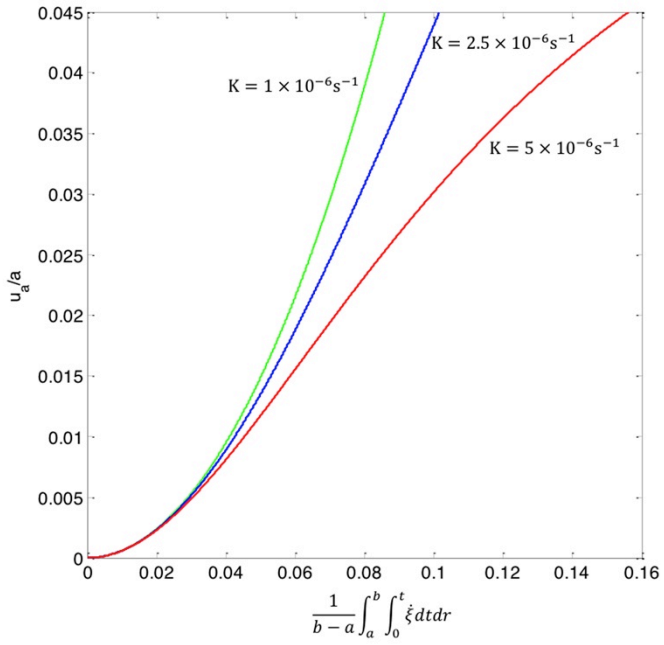

Figure 9: Influence of total mass removal on crack propagation

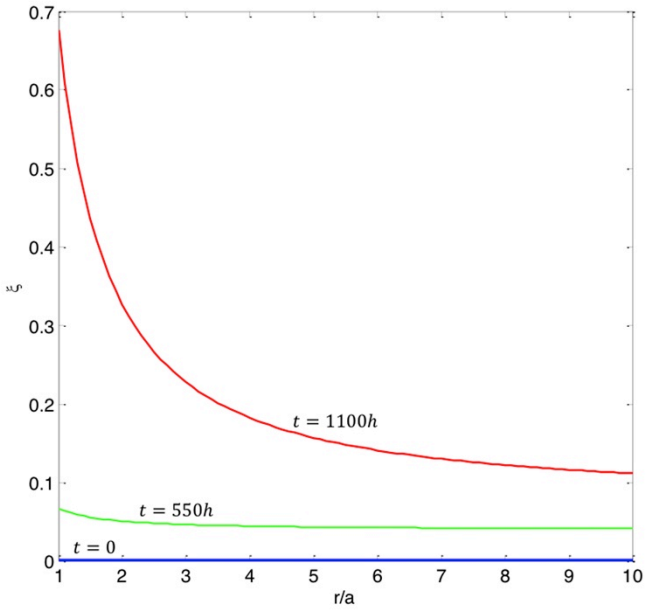

Figure 10: Evolution of the distribution of relative mass dissolution

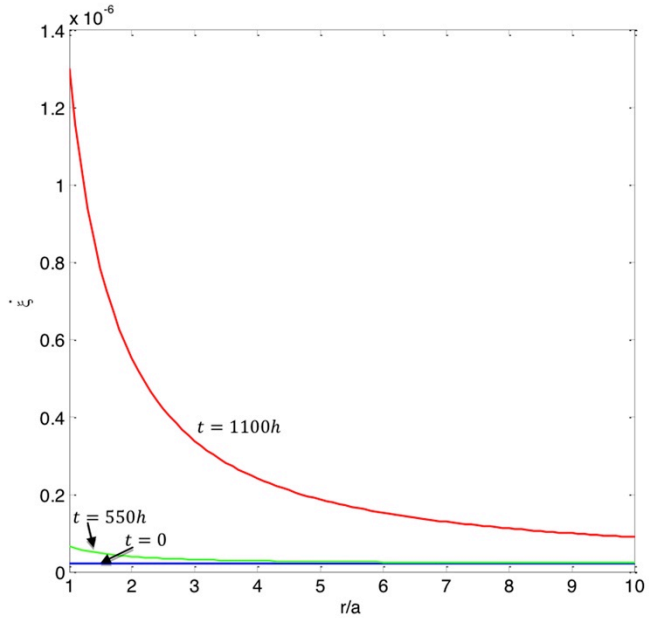

Figure 11: Evolution of the distribution of dissolution rate

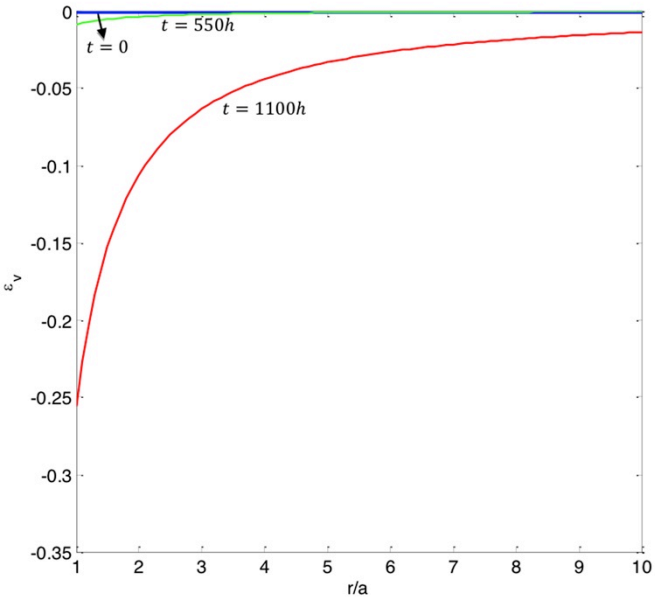

Figure 12: Evolution of the distribution of irreversible volumetric strain

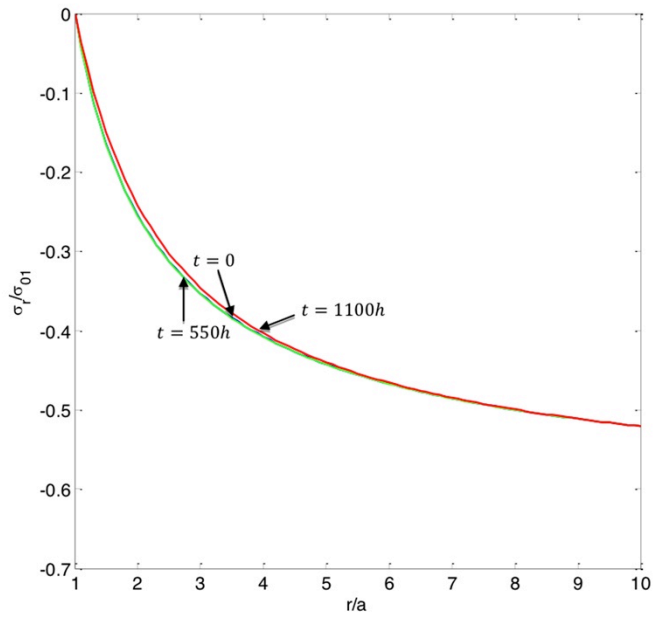

Figure 13: Evolution of radial stress distribution

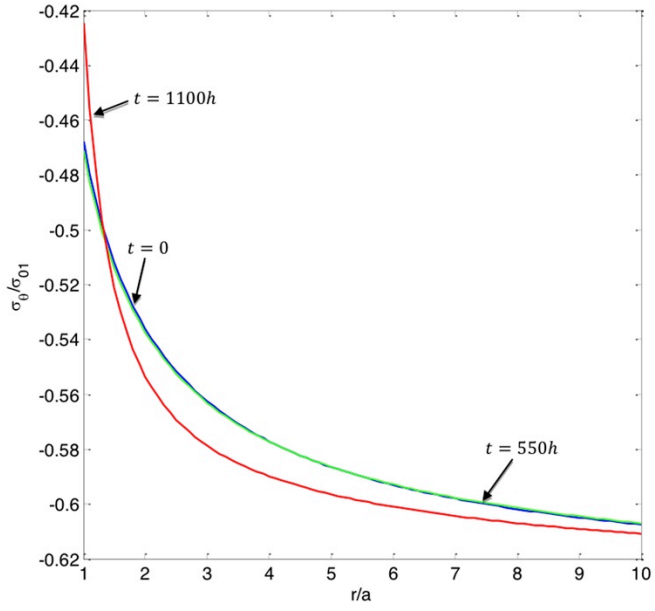

Figure 14: Evolution of circumferential stress distribution

5.2 Preliminary Results from Hydraulic Pressurizing Mode

The results obtained from Method I and Method II overlap well with each other, as shown in **Figure 15**, which provides us confidence for both results. The input parameters are $\alpha = 5$, $\beta = 1$, $\vartheta = \pi/6$, $tan\varphi = 0.2$, $b/a = 10$, $K_c = 1.0\times10^{-7}s^{-1}$, and K is set to be $1.0\times10^{-6}s^{-1}$ unless it is subject of a parametric study. Element refinements are performed and **Figure 15** is attained by 100 elements. In Method I, the total iteration number is only 198.

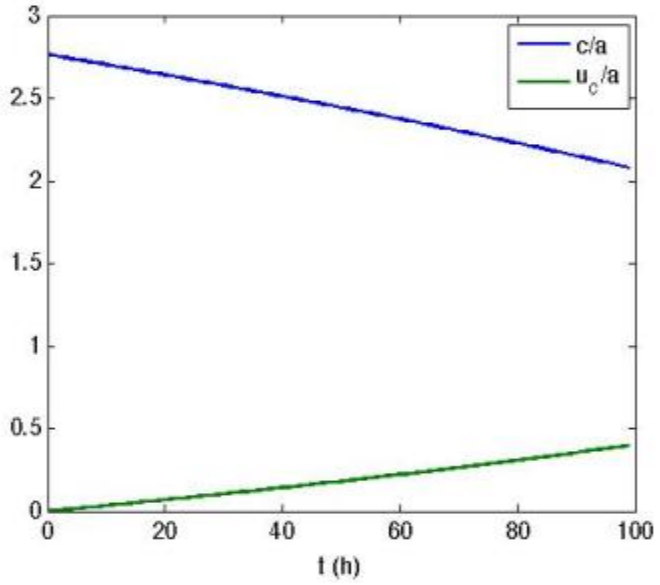

Figure 15: Non-dimensional interface position and the displacement at r = c

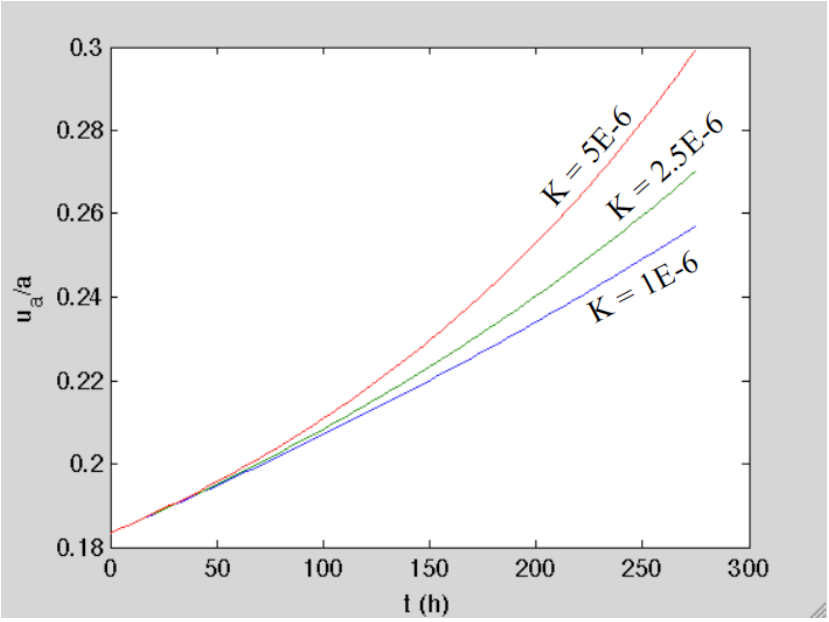

Figure 16: Crack propagation under variously intensified chemical environment

Since c and u_c are obtained, evolutions of the stress field, the strain filed, as well as the displacement of the crack tip, which is believed to a representative of crack penetration, can be revealed. The dimensionless form u_a/a is shown in **Figure 16** with various inputs of chemical intensity. As the value of chemical softening coefficient K, is increased by one order of magnitude the displacement u_a within 10 days start growing exponentially meaning accelerated crack propagation, which is physically an expected result of the damage-dissolution coupling. **Figure 17 ~ 19** show the evolutions of the volumetric strain, the radial and circumferential stress component distribution, respectively. Significant change of volumetric strains is confined in the near crack tip area. Because the radial stresses on both interior and exterior boundaries are fixed, hence there is little freedom for any evolution. However the distribution of σ_θ undergoes

noticeable evolution. The stress profile for each representative moment in the evolution is delineated in **Figure 6**, where A stands for stress state at the interior, B, B^1, B^2 represent the counterpart exterior, and C, C^1, C^2 denote the interface of the two zones, respectively.

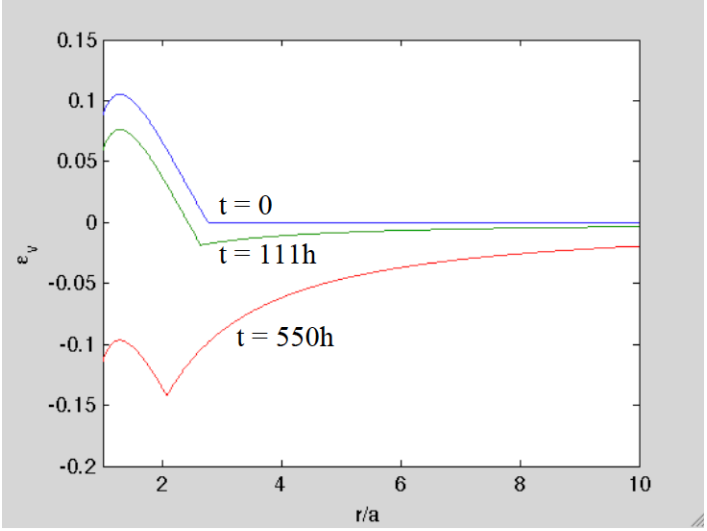

Figure 17: Evolution of volumetric strain along the radius

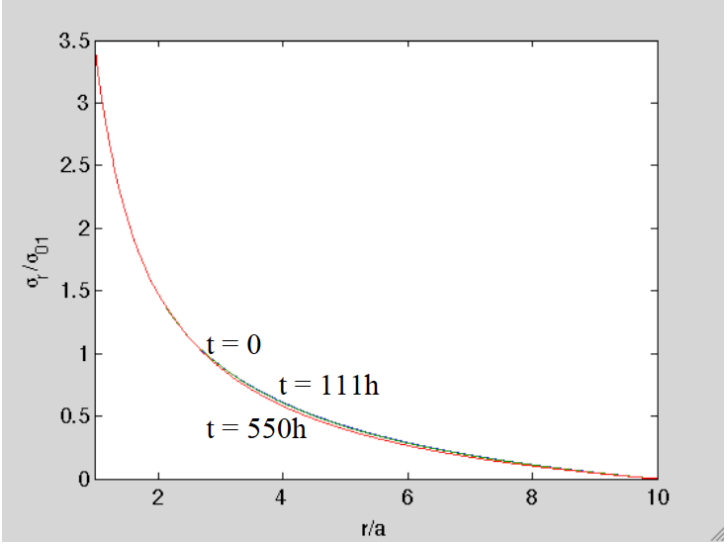

Figure 18: Evolution of radial stress along the radius

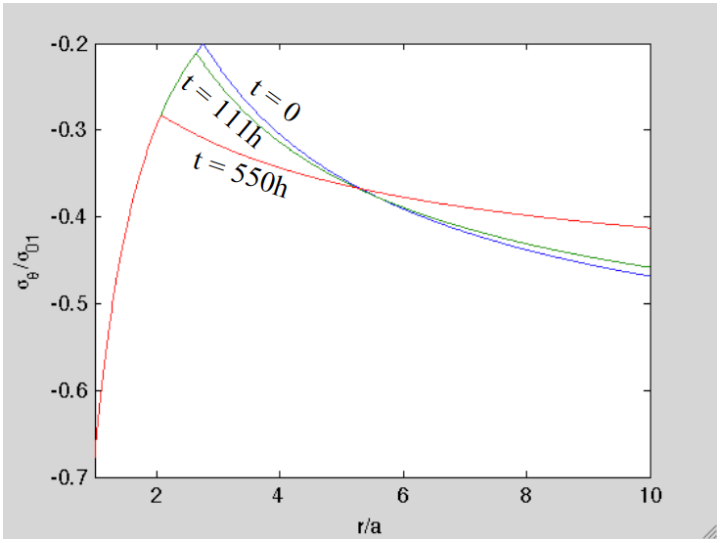

Figure 19: Evolution of circumferential stress along the radius

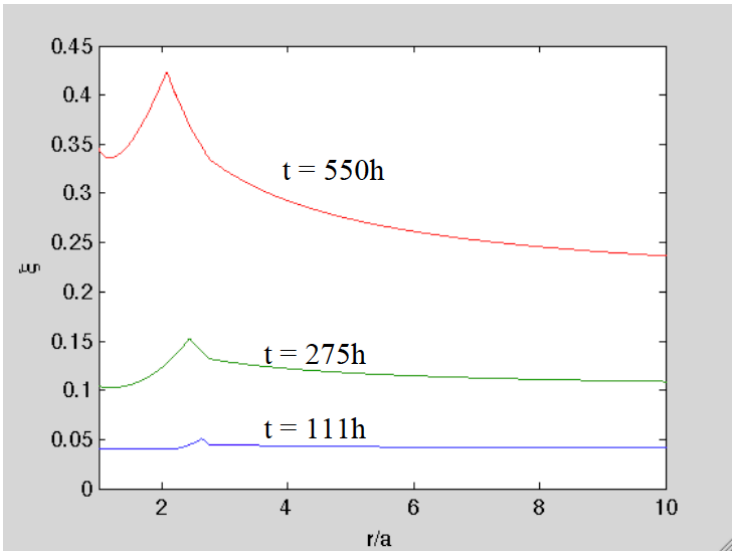

Figure 20: Evolution of the distribution of relative mass dissolution

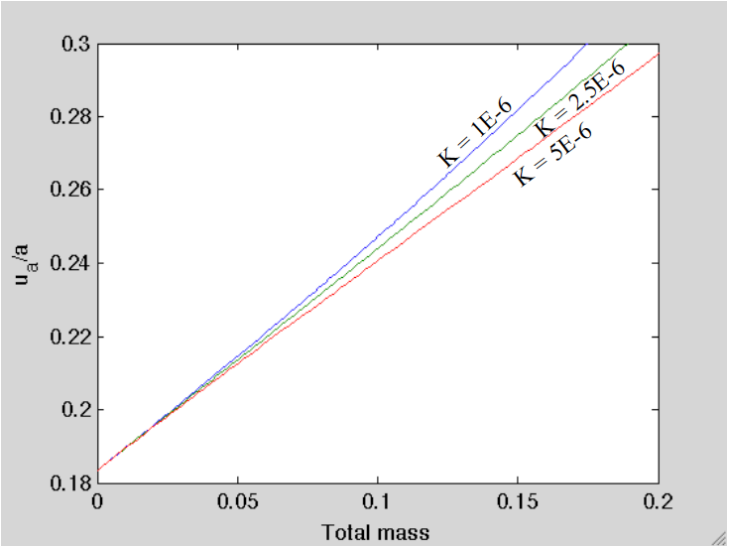

Figure 21: Influence of total mass dissolution on crack propagation

Shrinking of the critical-state zone is again observed. It is interesting to see that the dilatant zone can be further divided into two rings – in the inner ring the tensile circumferential stress increases, meaning the material is going through an overall hardening process; while in the outer ring the material softens. Significant softening only occurs near the exterior boundary, while the most significant hardening moves with $r=c$ towards the center of process zone. The evolution of the distribution of relative mass dissolution is presented in **Figure 20**. It is worth noting that the relative mass dissolution is significantly higher at the interface between the critical-state zone and the dilatant zone. **Figure 21** shows the influence of total mass dissolution (integration of dissolved mass on time and radius) on crack propagation with various inputs of chemical intensity. Rather than being exponential, the slop of the curves is almost linear,

which might indicate that dissolution in certain area within the process zone is not contributing much to the process of crack propagation as it is supposed to.

5.3 Damage-dissolution-diffusion

Inside the process zone, the phenomenon of diffusion occurs once the solute, i.e. calcite, is dissolved in water. The reference condition is set as a uniform dissolution at the surface of pre-existing voids within a REV. Interconnected voids within the process zone form micro-channels, providing pathways for calcite transport. At the crack tip, we assume that within the macro-pore, water washes away the excess of the mineral, and for simplicity we assume zero concentration, hence $x_{Ca^{2+}} = 0 \; at \; r = a$. The exterior of the process zone is an artificial boundary and is assumed to stay as it was at the initial state of the material, when dissolution was limited to the pre-existing micro-pores, hence $x_{Ca^{2+}} = x_0 \; at \; r = b$. An initial background steady-state diffusion field is created with the imposed boundary conditions.

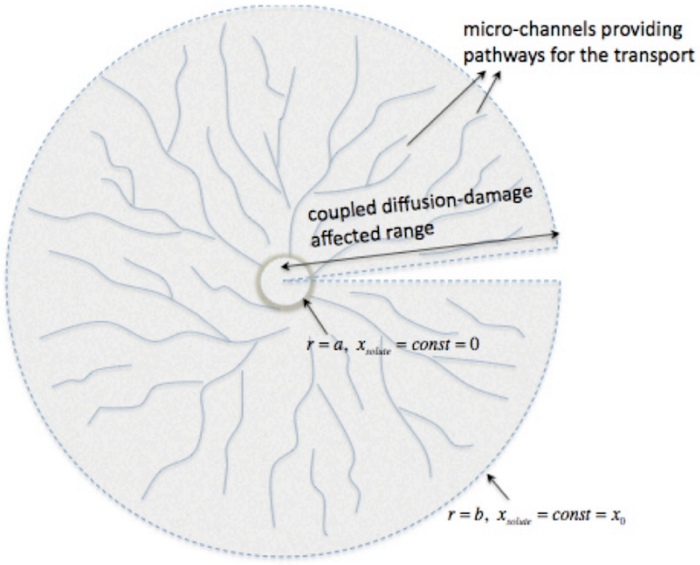

Figure 22: Coupled diffusion-damage-affected zone around the crack tip

The reactive diffusion is approximated as an axisymmetric field of concentrations (molar fraction of calcite) with uniformly a distributed sources (reaction sites) described by the following governing partial differential equation with given boundary conditions as well as the initial conditions.

$$\frac{\partial x_{Ca^{2+}}}{\partial t} = D\left(\frac{\partial^2 x_{Ca^{2+}}}{\partial r^2} + \frac{1}{r}\frac{\partial x_{Ca^{2+}}}{\partial r}\right) + k_+(\phi|\varepsilon_v(r,t)| + \phi_c), \tag{30}$$

where $x_{Ca^{2+}}$ is the molar fraction of calcium in the fluid phase within the process zone, and D represents the calcium diffusion coefficient, which is assumed a constant within the process zone. As it is seen in Eqn. (30), the source term depends on the amount of volumetric deformation, hence its solution is coupled to the solution of independent equations discussed previously.

The damage-affected zone of the material induces evolution of the concentration of solutes, coupled with the evolving deformation (micro-cracking). The distribution of mineral concentration and the flux of the solute mass are hence affected by solid mechanics of the problem. The diffusive flux at the inner boundary, representing the influence of the mechanical damage on the net dissolved mass, is of particular interest, and it can be correlated with the displacement of the crack tip, or crack propagation. **Figure 23** and **Figure 24** show the evolution of mass flux J_a at $r = a$, and its dimensionless counterpart. M is a coefficient representing the effect of deformation/damage associated with the dilatant volumetric strain on the mass transfer, $M = s\phi k_+ a^2/Dx_0$. $M = 0$ means a pure diffusion process without the presence of chemo-mechanical coupling. As indicated in both **Figure 23** and **Figure 24**, the reactive dissolution coupled with the irreversible damage of the medium, plays an important role in the diffusion processes. Finally, it is possible to set the crack propagation against the flux of the solute at the near tip perimeter, **Figure 25**. Since the total flux of mass removal is experimentally measurable, we shall be able to verify the simulation results against an experiment, and perform an *in situ* calibration.

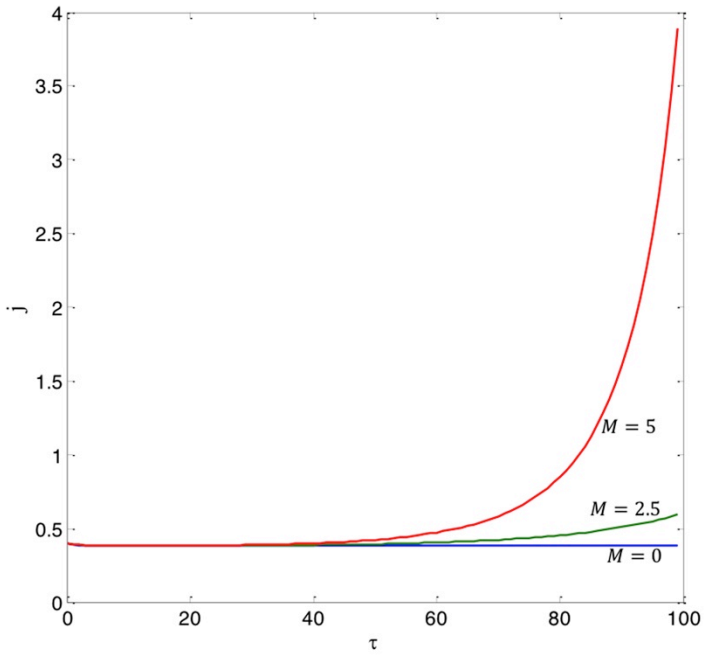

Figure 23: Evolution of the dimensionless mass flux at the crack tip

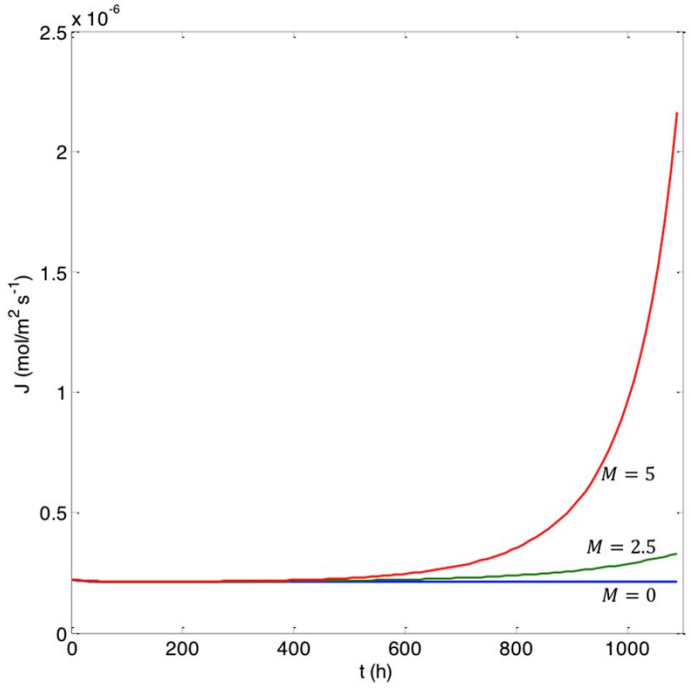

Figure 24: Evolution of the mineral mass flux at the crack tip

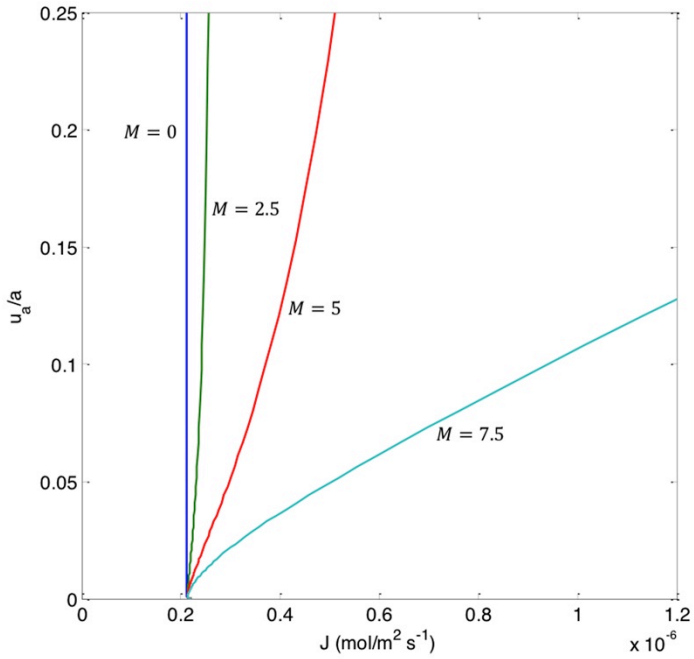

Figure 25: Correlation between the exiting mass flux and penetration of the crack tip

6. Conclusions and Discussion

A damage-enhanced reactive chemo-plasticity model was developed to describe simplified scenarios of chemically induced propagation, of an otherwise subcritical crack in a pre-stressed geomaterial. An open system was selected, meaning that the local precipitation is neglected, and chemical dissolution was considered as a form of mass removal. The chemo-plasticity coupling effect was investigated with an assumption of simple hardening rules, linear form of yield condition, rigid behavior prior to yielding. Still, a number of meaningful conclusions were reached. The results have demonstrated a significant role of the compensatory mechanism between strain hardening and chemical softening. It was possible to obtain the rate of crack propagation against time, total accumulated relative mass removal, and against the exiting mineral flux. Chemical softening intensity, dominating the rate of mineral dissolution has been proved essential to the progress of crack propagation, as well as that of soil/rock degradation.

Moreover, it is seen in both remote traction mode and hydraulic pressurizing mode, that with the mass removal, the rate of crack penetration initially substantially increases. Most importantly, this simplified model is able to demonstrate the compensatory mechanism between strain hardening and chemical softening in the material and to correlate the propagation of a single crack with the intensity and the location of chemical mass removal inside its process zone. The findings of this study

may be applied to several energy source harvesting areas including petroleum / natural gas and geo-thermal engineering (to such processes as acid enhanced hydraulic fracturing, reservoir engineering), as well as in the area of slope stability, etc., where the soil/rock mass is subjected to chemically induced degradation.

7. Future Work

- ***To address the concept of geochemo-hydrology and of hydro-geomechanics, and further perform a conceptual analysis on the coupling mechanisms in order to propose a model for chemo-hydro-geomechanical coupling in environmentally enhanced crack propagation.***

The chemo-mechanical processes related to chemical mass removal as discussed above are found in many situations where hydrological processes including fluid flow and solute transport through the rock mass take place as well. A comprehensive diagram, illustrating the inside mechanics in fully coupled chemo-hydro-mechanical processes, is presented in **Figure 26**. Dynamic fluid contributes to the material degradation via releasing mineral fines and weakening the rock matrix, as described in the concept of hydro-erosion; while the local intrinsic permeability of the rock is modified by the micro-channeling effect at the tips of cracks under chemo-mechanical loading. Meanwhile, mineral dissolution enlarges the aperture and hence enhances the local permeability as well. Local concentration of hydrogen alters as a result of diffusive-advective transport within the medium. Higher concentration of H+ intensifies chemical reactions as the dissolution rate is dependent on the local pH. Given pressure is fixed on the boundaries, flow velocity is linked to the change in porosity through dilatancy, and its magnitude determines whether the advection effect is significant in the transport process.

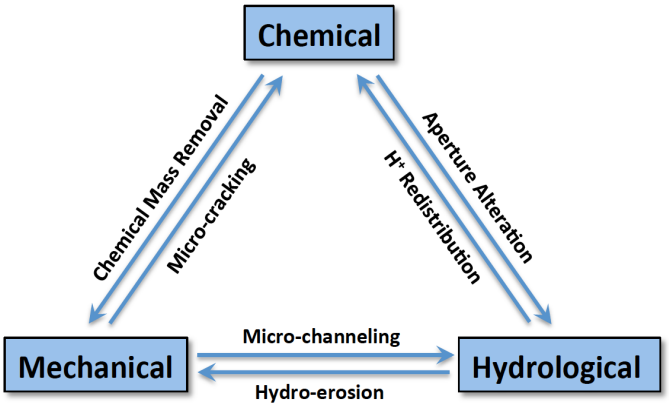

Figure 26: Inside mechanics in chemo-hydro-mechanical processes

Feedback mechanisms in this chemo-hydro-geomechanics will be explored in light of Hueckel and Hu (2009)'s work on sediment compaction (as shown in **Figure 27**). Scale analysis will also be performed, aiming at obtaining cross scale functions.

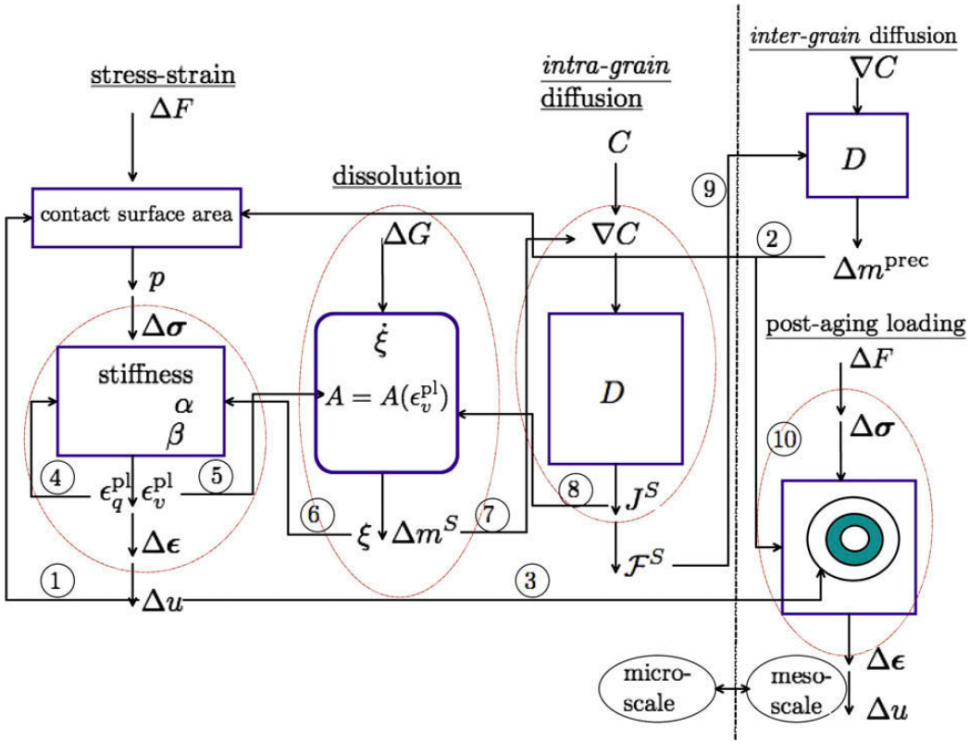

Figure 27: Representation of feedback mechanisms in the process of sediment compaction (Hueckel and Hu, 2009)

- ***To establish the coupling mechanics between hydraulic and chemo-geomechanical processes, especially the coupling between the two types of mass removal, i.e. chemical dissolution and hydro-erosion.***

Aperture function plays an important role in the coupling between hydraulic and mechanical processes (Tsang, 1991), however the link between alteration of aperture function and the process of mass removal has never been related.

Effective permeability of fractured rock media depends not only on the interconnected cracks, but also inter-crack solid rock generalized transmissivity between

adjacent unconnected cracks, especially when a large portion of fractures are non-connected. This transmissivity is a function of permeability of open cracks, intrinsic permeability of the rock matrix and the distance between adjacent crack tips. As a matter of fact, two neighboring cracks might function as "connected" if sufficient micro-channeling takes place between them (shown in **Figure 28**). Such phenomena may become pronounced when the pre-fractured material is stressed and is subject to mass loss due to chemical dissolution and hydro-erosion. As cracks propagate, the medium transmissity is most sensitive on the segments of lowest permeability, i.e. the area of solid matrix between two adjacent cracks. Removal and precipitation of mineral from the cracks themselves affects the permeability evolution (Hueckel and Hu, 2011).

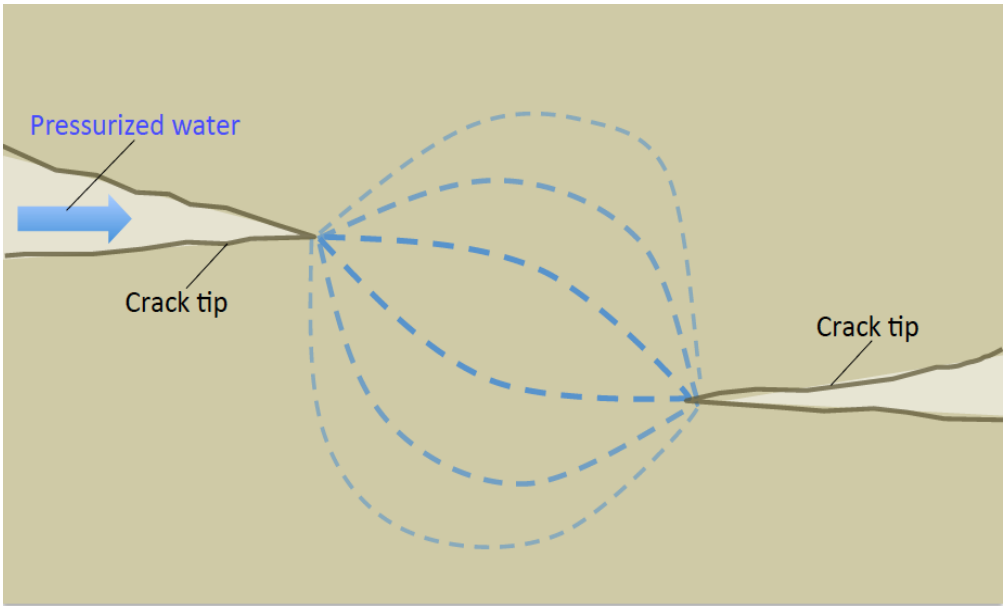

Figure 28: Illustration of micro-channeling between two adjacent cracks

Geometry representation of a simplified model for this bottle neck effect between two adjacent crack tips, is presented in **Figure 29**. The two cracks, i.e. inlet and outlet of the fluid flow, are represented by a convergent channel and a divergent channel respectively. The two channels are connected by a thin tube and its aperture depends on the permeability of solid matrix between the two adjacent cracks. As crack propagates, the convergent channel is enlarged, and increase in aperture function at this area can be related to the depth of crack penetration. Inside the mass removal affected zone, aperture changes with time, and is thereby denoted as $\delta_1(t)$. $\delta_1(t)$ is hence coupled with the process of mineral mass removal.

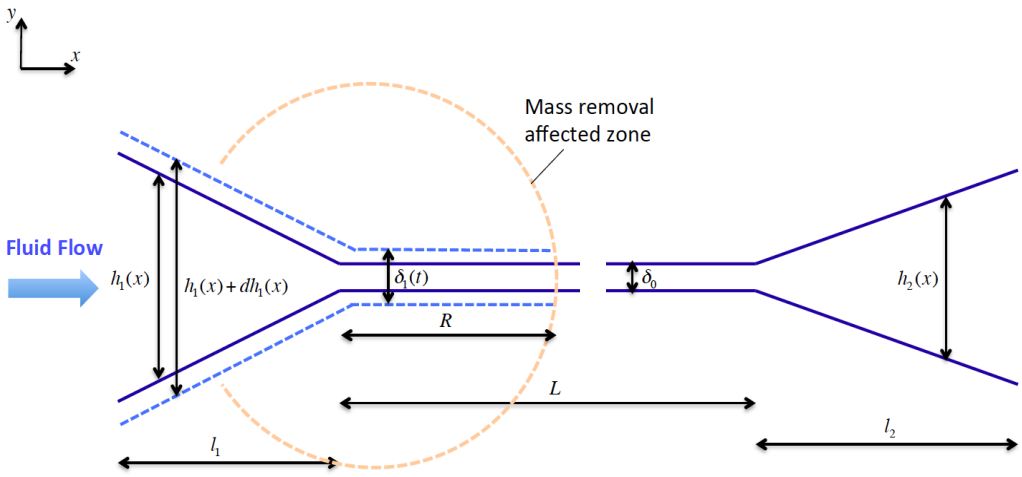

Figure 29: Geometry representation of a simplified model for crack bridging due to fluid flow

Hueckel et al. (1997) studied flow through divergent and convergent channels in their paper on fabric alteration and permeability changes in clay by contaminants. **Figure 30 (a, b)** show flow through a single divergent channel and an elementary cell with the large channel contributing with negligible resistance to flow and two smaller wedge-shaped channels. The mechanisms on crack bifurcation due to fluid flow will further be explored.

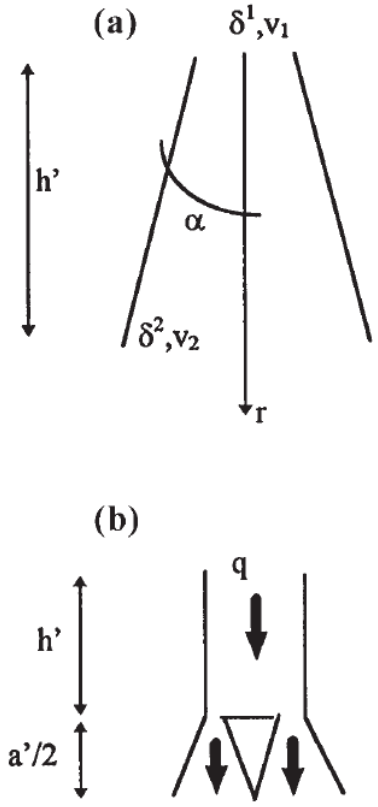

Figure 30: Flow through divergent channel: (a) notation for a single divergent channel; (b) an elementary cell with the large channel contributing with negligible resistance to flow and two smaller wedge-shaped channels. (Hueckel et al., 1997)

- ***To perform a series of experiments that simulate the geo-chemically and erosion enhanced crack propagation as well as the alteration of overall hydraulic transmissivity.***
- ***To investigate behaviors of fractures subject to aggressive aqueous environment under type II (shearing) mode.***

We shall further extend our investigation to the shearing mode of fracture as it has been suggested that failure of subcritical fractures due to shear displacement plays an important role in reservoir permeability enhancement by hydraulic fracturing. Experimentally, we would like to observe the behavior of a shear-induced subcritical fracture subject to aggressive aqueous environment and meanwhile under hydraulic load.

- ***To further explore the chemo-hydro-geomechanical coupling in a system of fractures.***

Explorations on a system of fractures in a geomaterial will focus on coupling the developed chemo-hydro-geomechanisms with a proper stochastic model for crack dimensions and distribution in a medium.

Bibliography

André, L., Audigane, P., Azaroual, M., & Menjoz, A. (2007). Numerical modelling of fluid-rock chemical interactions at the supercritical CO2 - liquid interface during supercritical CO2 injection into a carbonate reservoir, the Dogger aquifer (Paris Basin, France). *Energy Conversion and Management* **48**, No. 6, 1782-1797.

Bathurst, G. C. (1958). Diagenetic fabrics in some British Dinantian limestones. *Liverpool Manchester Geol J* **2**, 11-36. Bigoni, D. & Laudiero, F. (1989). The quasi-static finite cavity expansion in a non-standard elasto-plastic medium. *International Journal of Mechanical Sciences* **31**, No. 11-12, 825-837.

Carter, B. J., Desroches, J., Ingraffea, A. R., & Wawrzynek, P. A. (2000). Simulating fully 3D hydraulic fracturing. In *Modeling in geomechanics* (Zaman M., Booker J., & Gioda G. (ed.)). New York: Wiley Publishers.

Ciantia, M. O. & Hueckel, T. (2013). Weathering of stressed submerged calcarenites: chemo-mechanical coupling mechanisms, *Geotechnique*, *Proc. Bio- and Chemo-mechanical Processes in Geotechnical Engineering.*

Coffman, S. (2009). The Safety of Fracturing Fluids - A Quantitative Assessment. *Committee to Preserve the Finger Lakes*. Print.

Collins, I. F. & Stimpson, J. R. (1994) Similarity Solutions For Drained And Undrained Cavity Expansions In Soils, *Geotechnique* **44**, No. 1, 21-34.

Dershowitz, W., La Pointe, P., Parney, B., Cladouhos, T. (2001). Multiphase discrete fracture modeling in support of improved oil recovery from the North Oregon Basin, Wyoming. *38th US Rock Mechanics Symposium*, Washington DC. AA Balkema, Lisse, 663-668.

Dusseault, M. B. (2011) Geomechanical challenges in petroleum reservoir exploitation. *KSCE J Civ Eng* **15**, 669-678.

Gajo, A. Loret, B., Hueckel, T. (2002). Electro-chemo-mechanical couplings in saturated porous media: elastic–plastic behaviour of heteroionic expansive clays. *International Journal of Solids and Structures* **39**, No. 16, 4327-4362.

He, C., Guo, J., Wang, W., Liu, C. (2010). Study on acidizing wormhole of tight carbonate reservoir. *Duankuai Youqitian (Fault-Block Oil & Gas Field)* **17**, No. 2, 235-238.

Hori, M. & Nemat-Nasser, S. (1987). Interacting Micro-Cracks Near The Tip in the Process Zone of a Macro-Crack. *J. Mech. Phys. Solids* **35**, No. 5, 601-629.

Howard, G. C. & Fast, C. R. (1970). *Hydraulic Fracturing*. New York: Society of petroleum engineering of AIME.

Hueckel, T. & Mróz, Z. (1973). Some boundary value problems for variable density materials. *Problèmes de la Rhéologie, PWN , Warsaw,* 173-191.

Hueckel, T. (1992). Water–mineral interaction in hydro-mechanics of clays exposed to environmental loads: a mixture theory approach. *Can Geotechn J*. **29**, 1071-1086.

Hueckel, T. (1997). Chemo-plasticity of clays subjected to stress and flow of a single contaminant. *Int. J. Numer. Anal. Meth. Geomech* **21**, 43-72.

Hueckel, T., Pellegrini, R; Del Olmo C., (1998). A constitutive study of thermo-elastoplasticity of deep carbonatic clays. *International Journal for Numerical and Analytical Methods in Geomechanics* **22**, No. 7, 549-574.

Hueckel, T., Cassiani, G., Fan, T., Pellegrino, A., & Fioravante, V. (2001). Aging of oil/gas-bearing sediments, their compressibility, and subsidence. *J Geotechn Geoenviron Eng, ASCE* **127**, No. 11, 926-938.

Hueckel, T. (2002). Reactive plasticity for clays during dehydration and rehydration. Part I: concepts and options. *Int J Plast*. **18**, No. 3, 281-312.

Hueckel, T. & Pellegrini, R. (2002). Reactive plasticity for clays: application to a natural analog of long-term geomechanical effects of nuclear waste disposal. *Engineering Geology*. **64**, No. 2-3, 195-215.

Hueckel, T., Cassiani, G., Prevost, J. H., Walters, D. A. (2005). Field derived compressibility of deep sediments of the Northern Adriatic. In *Land subsidence. Special volume: Multi-disciplinary assessment of subsidence in the Ravenna area.* Rotterdam: Millpress, pp. 35-51.

Hu, L. B. & Hueckel, T. (2007 a). Creep of saturated materials as a chemically enhanced rate-dependent damage process. *Int. J. Numer. Anal. Meth. Geomech* **31**, 1537-1565.

Hu, L. B. & Hueckel, T. (2007 b). Coupled chemo-mechanics of intergranular contact: Toward a three-scale model. *Computer & Geotechnics* **34**, No. 4, 306-327.

Hueckel T. and Hu, L. B. (2009). Feedback mechanisms in chemo-mechanical multi-scale modeling of soil and sediment compaction, *Computers and Geotechnics* **36**, 934-943.

Jackson, R. B., Pearson, B. R., Osborn, S. G., Warner, N. R., and Vengosh, A. (2011). *Research and Policy Recommendations for Hydraulic Fracturing and Shale Extraction*. Center on Global Change, Duke University: Durham, NC.

Johnson, K. L. (1970). The correlation of indentation experiments. *J Mech Phys Solids*. **18**, 115-126.

Lin, Q. & Labuz, J. (2011). Process-Zone Length from image Analysis. *ARMA* **11**, 405-411.

Loret, B., Hueckel, T., Gajo, A. (2002) Chemo-mechanical coupling in saturated porous media: elastic–plastic behaviour of homoionic expansive clays. *International Journal of Solids and Structures* **39**, No. 10, 2773-2806.

Meredith, P. G. and Atkinson, B. K. (1983) Stress corrosion and acoustic emission during tensile crack propagation in Whin Sill Dolerite and other basic rocks. *Geophys J Astr* **75**, 1-21.

Mura, T. (1982). *Micromechanics of Defects in Solids*, Hague-Boston: Martinus Nijhoff.

Ostapenko, G. T. (1968). Recrystallization of minerals under stress. *Geochem Int.* **5**, 183-186.

Ostapenko, G. T. (1975). Theories of local and absolute chemical potential, their experimental testing and application of the phase rule to the systems with nonhydrostatically stressed solid phases. *Geochem Int.* **11**, 355-389.

Portier, S. & Vuataz, F. D. (2010). Developing the ability to model acid-rock interactions and mineral dissolution during the RMA stimulation test performed at the Soultz-sous-Forêts EGS site, France. *Comptes Rendus Geoscience* **342**, No. 7-8, 668-675.

Rahman, M. M. (2008). Constrained hydraulic fracture optimization improves recovery from low permeable oil reservoirs. *Energy Sources, Part A* **30**, 536-551.

Schmidt, R. A. (1980). A Microcrack Model And Its Significance to Hydraulic Fracturing And Fracture Toughness Testing. *The 21st U.S. Symposium on Rock Mechanics (USRMS)*, May 27 - 30, 1980 , Rolla, Missouri

Tada, R., Maliva, R., Siever, R. (1987). A new mechanism for pressure solution in porous quartzose sandstone. *Geochim Cosmochim Acta.* **51**, 2295-2301.

Taylor, K. C., Al-Ghamdi, A., Nasr-El-Din H. A. (2004). Effect of additives on the acid dissolution rates of calcium and magnesium carbonates. *Society of Petroleum Engineers Journal* **19**, 122-127.

Tsang, C. F. (1991). Coupled hydromechanical-thermochemical processes in rock fractures. *Reviews of Geophysics* **29**, 4, 537-551.

Zhao, Y., Duan, X. K., Hu, L.B., Cui P. and Hueckel, T. (2011). Multi-scale chemo-mechanical analysis of the slip surface of landslides in the Three Gorges, China. *Science in China Series E: Technological Sciences* **54**, No. 7, 1757-1765.

Zimmermann, G., Blöcher, G., Reinicke, A., Brandt, W. (2011). Rock specific hydraulic fracturing and matrix acidizing to enhance a geothermal system - Concepts and field results. *Tectonophysics* **503**, No. 1–2, 146-154.